7

Thermohaline intrusions

As is the case for the majority of key double-diffusive effects, the modern theory of thermohaline intrusions was launched by Melvin Stern. Using stability arguments, Stern (1967) predicted a tendency for the spontaneous generation of intrusive quasi-horizontal structures, spreading across lateral temperature and salinity fronts in a double-diffusive fluid. Stern's theory was guided by observations (Stommel and Fedorov, 1967) of "hundreds of superimposed laminae from 2–30 meters thick," coherent over large horizontal distances and readily identifiable in the vertical temperature and salinity casts in the main thermocline of the Timor Sea (Fig. 7.1). While Stommel and Fedorov (1967) could not precisely identify their origin, they hypothesized that intrusions might be "direct evidence of the more exotic types of two-diffusivity convection." One cannot help being equally impressed by the shrewd comment of Stommel and Fedorov, which seems to have been based entirely on their physical intuition, and by Stern's ability to develop a consistent intrusion model from such a subtle observational hint.

In the years following Stern's discovery, thermohaline intrusions continued to attract steady interest from oceanographers and applied mathematicians. The motivation to understand and predict intrusion properties comes from the necessity to quantify their role in the lateral mixing of oceanic water masses. A fundamental problem of physical oceanography is to explain how the differential thermodynamic forcing of the sea-surface – heating in the tropical regions and high-latitude cooling – is balanced by advective and mixing processes in the ocean interior (Wunsch and Ferrari, 2004; Song *et al*., 2011). Ultimately, the temperature and salinity variances are dissipated by molecular diffusion acting on the microscale, with larger-scale processes playing a catalytic role in the chain of mixing events (e.g., Merryfield, 2005). While the dynamic connection between basin-scale forcing and microscale mixing has not been fully explained, plausible scenarios have been proposed and considered. Garrett (1982) suggested that an essential component of the global T–S cascade to small scales involves thermohaline interleaving. This

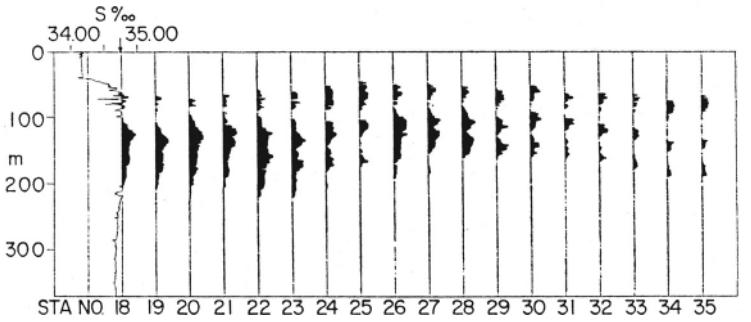

Figure 7.1 One of the first observations of thermohaline intrusions. Salinity profiles taken off Mindanao reveal multiple inversions laterally correlated between stations, taken as evidence of active interleaving of the adjacent water masses. From Stommel and Fedorov (1967).

sentiment was echoed by a number of oceanographers (Schmitt, 1994b; Ruddick and Kerr, 2003; Song *et al.*, 2011) but is in dire need of corroboration and quantification. A major predicament in this regard is caused by our limited understanding of processes controlling the intensity of intrusive mixing. Even such fundamental mixing characteristics as typical lateral eddy diffusivities due to intrusions are poorly known, with estimates reported in the literature varying by several orders of magnitude. Despite the general acceptance of its importance, no attempt has been made to incorporate interleaving into General Circulation Models, yet another sign of the challenges and uncertainties facing the community. Double-diffusion is not for weaklings; it requires the patience of a saint and the intensity of a Rottweiler. On the positive side, a host of unresolved interleaving problems opens numerous opportunities for significant advancement of this field – the opportunities that readers of our monograph are encouraged to pursue.

For pedagogical reasons, in the next section (Section 7.1) we present the linear theory of thermohaline interleaving in its most basic form: the model excludes the effects of planetary rotation, baroclinicity and ambient forcing. The most common generalizations of the stability analysis are considered in Section 7.2. While linear theory by itself cannot quantify the magnitude and transport characteristics of intrusions, it explains their spatial patterns and offers valuable physical insights. Discussion of the fundamentally nonlinear properties of intrusions follows shortly after (Section 7.3).

7.1 Linear theory

While intrusions can be produced by several mixing mechanisms (salt fingering, diffusive convection, differential diffusion, molecular diffusion or a combination

thereof) we focus on finger-driven interleaving. Our starting point is the Boussinesq equations of motion, applied to the large-scale, relative to fingers, flow components. The basic state is assumed to be at rest ($\bar{\vec{v}} = 0$), whereas the temperature and salinity fields are separated into the linearly stratified basic state $(\bar{T}, \bar{S})$ and a departure (T', S') from it. In the intrusion problem, it becomes essential to include small but finite horizontal gradients, which for simplicity are assumed to be uniform and density compensated. That is, the basic density field is horizontally homogeneous. Without loss of generality, the x and y axes are oriented in the cross-front and along-front directions respectively ($\alpha\bar{T}_x = \beta\bar{S}_x > 0, \alpha\bar{T}_y = \beta\bar{S}_y = 0$). To reduce the number of governing parameters, we employ the standard double-diffusive system of non-dimensionalization (1.11) and linearize the result:

$$\begin{cases} \frac{\partial T'}{\partial t} + Gu' + w' = -\frac{\partial F_T'}{\partial z}, \\ \frac{\partial S'}{\partial t} + Gu' + \frac{w'}{R_\rho} = -\frac{\partial F_S'}{\partial z}, \\ \frac{1}{Pr}\frac{\partial}{\partial t}\vec{v}' = -\nabla p' + (T' - S')\vec{k} + \nabla^2\vec{v}', \\ \nabla \cdot \vec{v}' = 0, \end{cases} \tag{7.1}$$

where (F_T', F_S') are the perturbations of temperature and salinity fluxes due to salt fingers and $G = \bar{T}_x$ is the non-dimensional horizontal temperature gradient, representing the slope of isotherms in the basic state. Following the mainstream approach (Stern, 1967; Toole and Georgi, 1981; Walsh and Ruddick, 1995, 2000; Smyth and Ruddick, 2010) the vertical T–S transport is parameterized as a function of local gradients as in (6.2). At this point, no attempt is made to take into account eddy momentum transport since the salt-finger Reynolds stress is typically much less than molecular friction (e.g., Stern *et al.*, 2001; Krishnamurti, 2006). Note that the opposite is true for the transport of heat and salt, which is dominated by the eddy fluxes; weak molecular dissipation can be either neglected or incorporated into the eddy fluxes (F_T, F_S).

As in the case of collective instability (Chapter 6), the parametric intrusion model requires users to assume specific flux laws in (7.1). The first models of this nature (Stern, 1967; Toole and Georgi, 1981) used the eddy diffusivity of salt (K_S), which is independent of density ratio (R_ρ). The realization that double-diffusive transport is significantly R_ρ-dependent has led to improved versions (Walsh and Ruddick, 1995, 2000; Merryfield, 2000; Smyth and Ruddick, 2010) that assume various ad hoc expressions for (F_T, F_S). The following examples are based on the most recent parameterization (3.10) derived from a suite of high-resolution direct numerical simulations (Radko and Smith, 2012). As previously (cf. Chapter 6), we analyze stability using normal modes (2.1), substitution of which in (7.1) yields the cubic growth rate equation analogous to (6.9), except that its coefficients are now also affected by lateral T–S gradients (G).

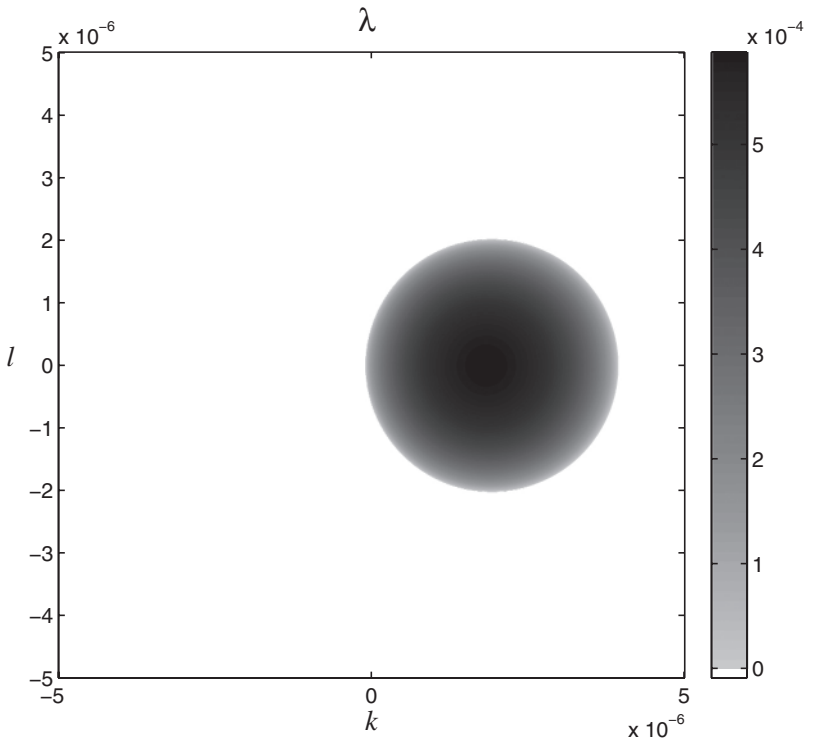

Figure 7.2 The growth rate (λ) of the salt-finger-driven intrusions as a function of (non-dimensional) horizontal wavenumbers k and l. Only the positive values of λ are shown. The largest growth rates are obtained for intrusions oriented across the front and tilted in the same sense as isotherms and isohalines.

In order to discriminate monotonically growing intrusive solutions from the oscillatory collective instability modes, we consider only real solutions of the growth rate equation. In Figure 7.2, the growth rate is plotted as a function of the horizontal wavenumbers (k, l) for a fixed value of the vertical wavenumber $m = 2\pi H^{-1}$; $H = 10^3$ (corresponding to $H_{\rm dim} \sim 10\,{\rm m}$) and the horizontal gradient $G = 0.001$. Two features of the growth rate pattern in Figure 7.2 are most noteworthy. First, the maximal growth rates are achieved for modes oriented across the front ($l = 0$), which is a generic property of intrusions in a non-rotating model. This property considerably simplifies the stability analysis, justifying the focus of most intrusion models on two-dimensional (x, z) dynamics. Another key observation is that positive growth rates are realized mostly for $k > 0$. This means that intrusions are spreading in a manner indicated in the schematic diagram in Figure 7.3 – warm and salty waters rise across the density surfaces, whereas the cold and fresh ones sink.

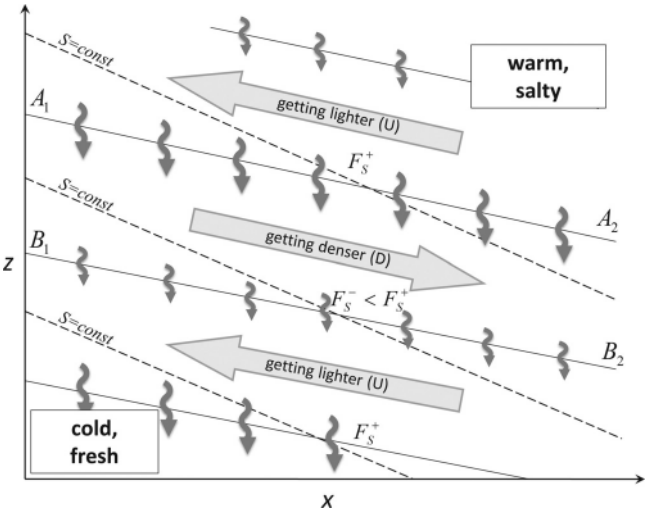

Figure 7.3 Illustration of the physical mechanism of thermohaline interleaving. The instability is driven by the positive feedback between changes in stratification caused by the interleaving and the resulting salt-finger buoyancy forcing, which further accelerates the intrusions.

In Figure 7.4, we plot the growth rates of the cross-front intrusions (recall that those are the most unstable ones) as a function of the intrusion slope $s = -\frac{k}{m}$ for various values of intrusion height. For typical oceanic conditions ($H_{\text{dim}} \sim 10\,\text{m}$, $G \sim 0.001$, $R_\rho \approx 2$) growth periods of several days are expected on the basis of linear theory. Generally, intrusions tend to grow slower than collective instability waves. This, however, does not imply that intrusions are less important. What makes intrusions ultimately more effective in modifying the background field is the persistence of their spatial pattern. Unlike collective instability waves, which periodically reverse the direction of the flow and thus partially negate the modification of the environment during an earlier phase, intrusions operate in the direct mode. They consistently transfer warm and salty fluid laterally into colder and fresher regions and vice versa, which results in strong down-gradient lateral mixing. In the vertical direction, the temperature and salinity fluxes on the intrusion scale are up-gradient (see Fig. 7.3), thereby opposing the microscale fluxes by salt fingers.

Physical interpretation

The monotonic growth of intrusions and their spatial orientation can be rationalized as follows. Consider a configuration (Fig. 7.3) in which fronts of the intrusive currents are tilted in the same sense as the temperature and salinity contours, sloping

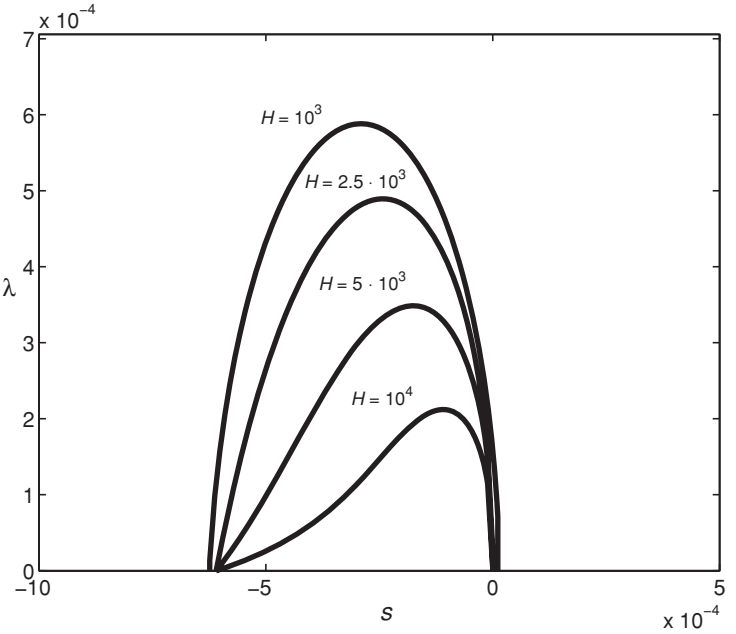

Figure 7.4 The non-dimensional growth rates (λ) of the cross-front intrusions as a function of slope for various values of intrusion thickness (H).

downward in the positive x-direction. However, the intrusions are tilted less than isotherms and isohalines. Thus, the upward-flowing intrusions (U in Fig. 7.3) advect warm and salty water across the isohalines and isotherms, resulting in a local increase of temperature and salinity. The downward intrusions (D in Fig. 7.3) reduce temperature and salinity by advecting relatively cold and fresh water. This perturbation pattern implies that the vertical temperature and salinity gradients (T_z, S_z) are enhanced in the regions below (above) the upward (downward) flowing intrusions – such as the (A_1, A_2) front shown in Figure 7.3. On the (B_1, B_2) front, located above the intrusion U and below the intrusion D, vertical temperature and salinity gradients are reduced. Higher (lower) T–S gradients, in turn, imply higher (lower) vertical salt-finger fluxes. Thus, the vertical T–S fluxes in the downward-moving intrusions converge, adding more heat and salt to the fluid. In the upward intrusions, fluid becomes fresher and colder due to salt fingers. What about density? The haline component of density flux in the salt finger environment exceeds its temperature component ($\gamma < 1$) and therefore the pattern of density perturbation is controlled by the convergence of the salinity flux. As a result, the density of the fluid in the downward intrusions (D) continuously increases, reinforcing their initial motion. The upward intrusions (U) become lighter due to the salt-finger fluxes, and further accelerate their ascent. This positive feedback mechanism explains the

monotonic growth of intrusions predicted by formal stability analysis. The negative sign of the intrusion slope is essential – an attempt to reproduce the foregoing argument for perturbations tilted with positive slope suggests suppression of such modes by the salt-finger fluxes.

Note that the physical description in Figure 7.3 pertains to finger-driven intrusions. If stratification and vertical mixing are predominantly diffusive (cold and fresh water on top of warm and salty) then the eddy density flux is dominated by its thermal, rather than haline, component: thermal stratification is the ultimate source of energy for diffusive convection and therefore $\gamma^* < 1$. Hence, the salt flux convergence argument proposed for the finger-driven intrusions (Fig. 7.3) has to be reversed. Diffusive intrusions tilted as shown in Figure 7.3 would be damped by the convergence of thermal fluxes, whereas intrusions with positive slope (warm and salty water sinking, cold and fresh rising) would grow. The spatial orientation of intrusions, diffusive and finger-driven, anticipated on the basis of qualitative physical arguments (Fig. 7.3) is consistent with the laboratory experiments on interleaving (e.g., Turner and Chen, 1974; Turner, 1978) and with the majority of oceanographic field measurements (reviewed in Section 7.6).

Two instructive comparisons should be made at this point. First, we highlight the dynamic differences and similarities between finger-driven and laminar (see Chapter 2) intrusions. While their physical mechanisms are analogous, the key difference is that for laminar fluids, temperature is the faster diffuser and salinity is the slower one. In this case, the vertical density flux is controlled by the diffusion of heat and perturbations oriented as in Figure 7.3 would be damped. Convergence of heat flux in the downward-moving regions (D) would make fluid lighter – and in the upward-moving regions denser – opposing the initial tendency and thus precluding the direct instability modes. Therefore, the preferred orientation of laminar intrusive modes is opposite to that in Figure 7.3: warm and salty intrusions sink, not rise, across density surfaces.

A second comparison can be made between intrusions (Fig. 7.3) and collective instability waves (Fig. 6.3). Both instabilities are driven by feedbacks between changes in the stratification and in the salt-finger fluxes. What makes intrusive dynamics special is the geometry of the system. In both models (Fig. 6.3 and Fig. 7.3) temperature and salinity increase upward at a given (x, y) location. However, the presence of horizontal temperature and salinity gradients, no matter how weak, makes it possible for a fluid parcel to rise and still end up in a fresher environment, which is an essential element of intrusion mechanics (Fig. 7.3). For this to occur, the parcel has to be displaced at very small angles to the horizontal – less than the slopes of isohalines. Using terminology introduced in studies of the baroclinic instability (Eady, 1949), we can claim that a necessary condition for interleaving is the presence of the "instability wedge" between the isohalines and

horizontal surfaces. Displacements of parcels within this instability wedge can be reinforced (Fig. 7.3); displacements outside of it are countered by the salt-finger fluxes. Thus, spontaneous interleaving cannot occur in horizontally homogeneous systems, where the instability wedge is absent. In the horizontally stratified fluid, on the other hand, both collective and intrusive modes can be present simultaneously. The perturbations oriented within the instability wedge engage the direct intrusive dynamics. Those outside of the instability wedge experience adverse forcing and therefore are either stable or overstable; the latter produce the familiar (Chapter 6) collective instability waves.

The γ-instability

An important aspect of the parametric intrusion model concerns its sensitivity to the assumed flux-gradient laws. Despite considerable progress in representing double-diffusive transport in smooth-gradient configurations (Chapter 3), the generally accepted and observationally validated flux-gradient laws are still lacking. Does the choice of parameterization really matter in terms of predicting the general properties of intrusions? In some cases, it does. Development of a flux-gradient model for double-diffusive fluids necessarily involves parameterizations of both heat and salt diffusivities. Equivalently, one can parameterize diffusivity of one component – say, salt diffusivity $K_S(R_\rho)$ – and the flux ratio $\gamma(R_\rho)$. The model solutions are sensitive to changes in both $K_S(R_\rho)$ and $\gamma(R_\rho)$. For instance, increasing the variation in diffusivity with density ratio tends to intensify interleaving. This effect can be readily rationalized by modifying the physical interpretation of intrusive instability in Figure 7.3. Intrusions modulate not only T–S gradients but the density ratio as well. When K_S decreases with R_ρ, the density ratio effect strengthens the positive feedback of the salt-finger fluxes on the intrusion. Taking into account variations in diffusivity can increase the intrusion growth rates by as much as a factor of four relative to the uniform K_S model (Walsh and Ruddick, 1995).

However, it is the flux ratio model that can affect some of the most fundamental intrusion characteristics (Walsh and Ruddick, 2000). The sensitivity of intrusions to the choice of $\gamma(R_\rho)$ relation is illustrated in Figure 7.5, where we plot the growth rate of the cross-front ($l = 0$) intrusions as a function of k and m. For the calculation in Figure 7.5a, we use the parameterization (3.10). A seemingly subtle modification is made in Figure 7.5b: we retain the parameterization of $K_S(R_\rho)$ but the flux ratio is set to a constant $\gamma_0 = \gamma(\bar{R}_\rho)$, where $\bar{R}_\rho$ is the density ratio of the basic state. At first, the result of this modification appears to be most dramatic. In Figure 7.5a, the growth rates are significantly larger than in Figure 7.5b, increasing without bound with m, and the unstable modes occupy a larger fraction of the wavenumber space. Such an extreme sensitivity of the parametric model to the

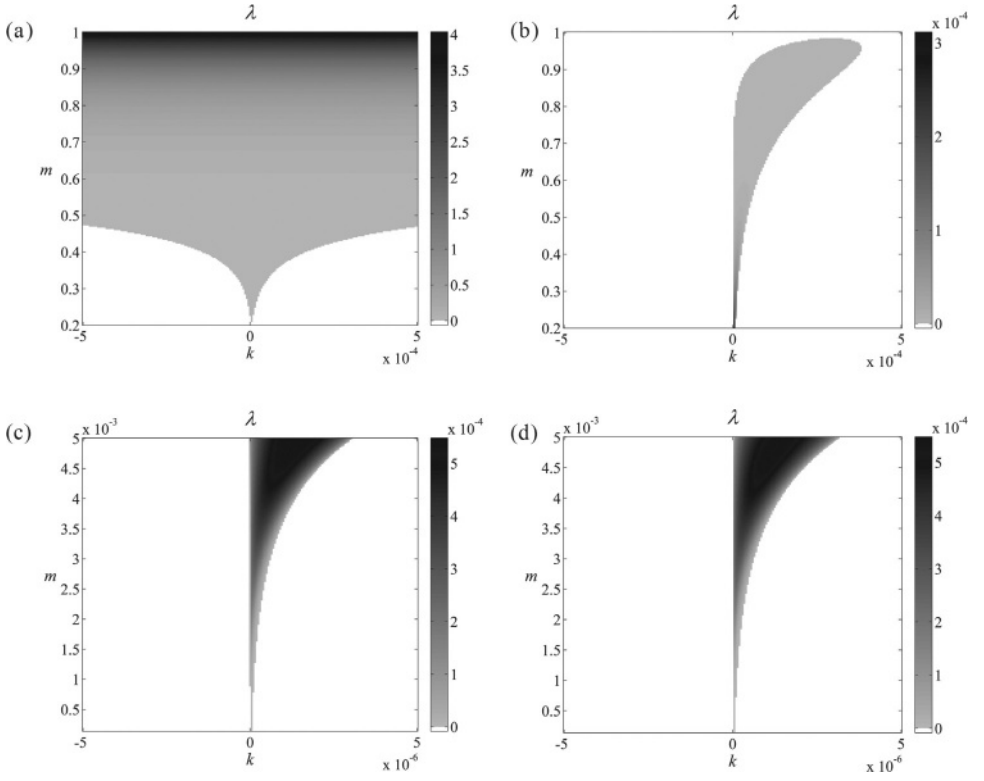

Figure 7.5 Significance of the variation in the salt-finger flux ratio for thermohaline interleaving. The growth rate is plotted as a function of the horizontal (cross-frontal) and vertical wavenumbers. The only difference between the calculations in (a) and (b) is that the former takes into account variation in flux ratio and the latter ignores it. However, the two calculations become similar when relatively small scales ($m > 5 \cdot 10^{-3}$) are excluded from consideration in (c) and (d).

assumed pattern of $\gamma(R_\rho)$ is a cause for concern, particularly since this dependence is not well constrained by lab experiments and field observations. The situation, however, does not look as bleak if we consider only the range of the parameter space occupied by relatively large-scale modes (Fig. 7.5c,d) with $m < 5 \cdot 10^{-3}$, which corresponds to a dimensional intrusion thickness of $H_{\text{dim}} \geq 10$ m. On such scales, both models, the R_ρ-dependent one in Figure 7.5c and the uniform γ model in Figure 7.5d, are mutually consistent.

Thus, taking into account the decreasing dependence of γ on R_ρ, which is expected for relatively low density ratios, reveals new instability modes. These modes are characterized by large growth rates and relatively small spatial scales and will be referred to as the γ-instability modes. Note that a majority of theoretical intrusion models (Stern, 1967; Toole and Georgi, 1981; Merryfield, 2000; among

others) assume constant flux ratio, thereby a-priori excluding the γ-instability from consideration. As a result, little is known about its dynamics and large-scale consequences, although preliminary evidence suggests that the γ-instability could have a substantial impact on the double-diffusive environment. Unlike conventional intrusive modes, the γ-instability is not contingent on the presence of lateral stratification and therefore it can potentially affect broader regions of the world ocean. The tendency of the γ-instability to operate on relatively small vertical scales complicates its representation in models and the assessment of its impact. Parametric models necessarily assume a substantial scale separation between individual salt fingers and phenomena that those models strive to represent. For relatively large-scale intrusions ($H_{\mathrm{dim}} \sim$ 10–100 m in the oceanographic context) this assumption is undoubtedly valid. Whether or not the smaller-scale γ-instability modes can be accurately described by parametric models depends on a particular configuration and therefore has to be answered on a case-by-case basis.

Preferred scales

The parametric model makes it possible to predict several key intrusion characteristics – the growth rate, slope, T–S amplitude ratio, and thickness – which are routinely measured in laboratory and field experiments. This opens an attractive opportunity to test and validate the model. As is conventional in instability theories, such predictions are based on the analysis of the most unstable modes. The underlying philosophy of such an approach ascribes a critical selective advantage to the modes with maximal growth rates. In the absence of strong biases in the initial amplitude, the rapidly growing perturbations are expected to dominate their slower growing counterparts during the initial phase of linear growth and thus control the flow pattern of the fully developed state as well. The application of this principle to the intrusion problem is not straightforward. Formally, the largest growth rates are attained by the small-scale γ-instability modes. The relation of these modes to the observed intrusions, which typically have much larger scales, is questionable. In order to exclude from consideration the γ-instability modes, we temporarily adopt the uniform flux ratio model as used for the calculation in Figure 7.5b,d.

The order-of-magnitude estimates of basic intrusion characteristics (thickness, growth rate and slope) can be obtained using scaling analysis of the parameterized system without detailed knowledge of the double-diffusive flux-gradient laws. For instance, Toole and Georgi (1981) suggest an explicit scaling relation for the (dimensional) intrusion thickness:

$$H_{\mathrm{TG}} \sim \left(\frac{\sqrt{\nu K_T}}{N} \frac{\bar{S}_z}{\bar{S}_x} \right)^{\frac{1}{2}}, \tag{7.2}$$

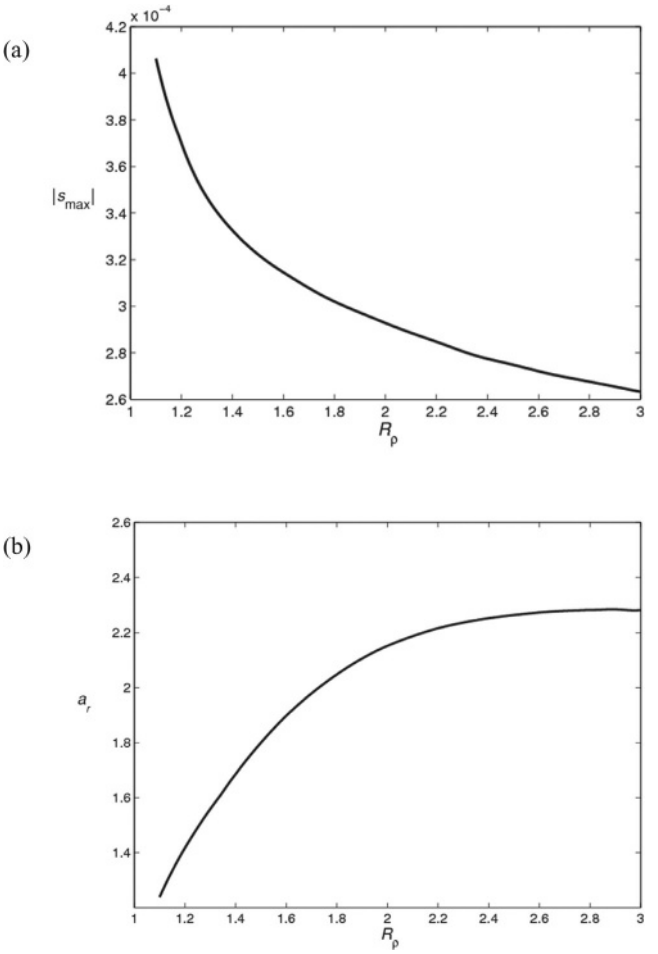

Figure 7.6 The slope (a) and the temperature/salinity amplitude ratio (b) of the most rapidly growing intrusion as a function of density ratio (R_ρ).

where $N = \sqrt{-\frac{g}{\rho}\frac{\partial \rho}{\partial z}}$ is the buoyancy frequency. The corresponding intrusion growth rate scales as $\lambda_{\mathrm{TG}} \sim K_T / H_{\mathrm{TG}}^2$. The molecular viscosity ν in (7.2) should be replaced by the eddy viscosity (K_M) for situations in which the latter dominates.

To be more quantitative, it becomes necessary to assume specific parameterizations of the vertical double-diffusive transport. For consistency, we shall continue to use the flux law (3.10). The experiments in Figures 7.6 and 7.7 examine the dependencies of the linear intrusion characteristics – slope, *T*–*S* amplitude ratio, growth rate and thickness – on the density ratio for a fixed value of the horizontal gradient ($G = 0.001$). The sensitivity to R_ρ is limited. The magnitude of the preferred slope (Fig. 7.6a) weakly decreases with density ratio, while the orientation

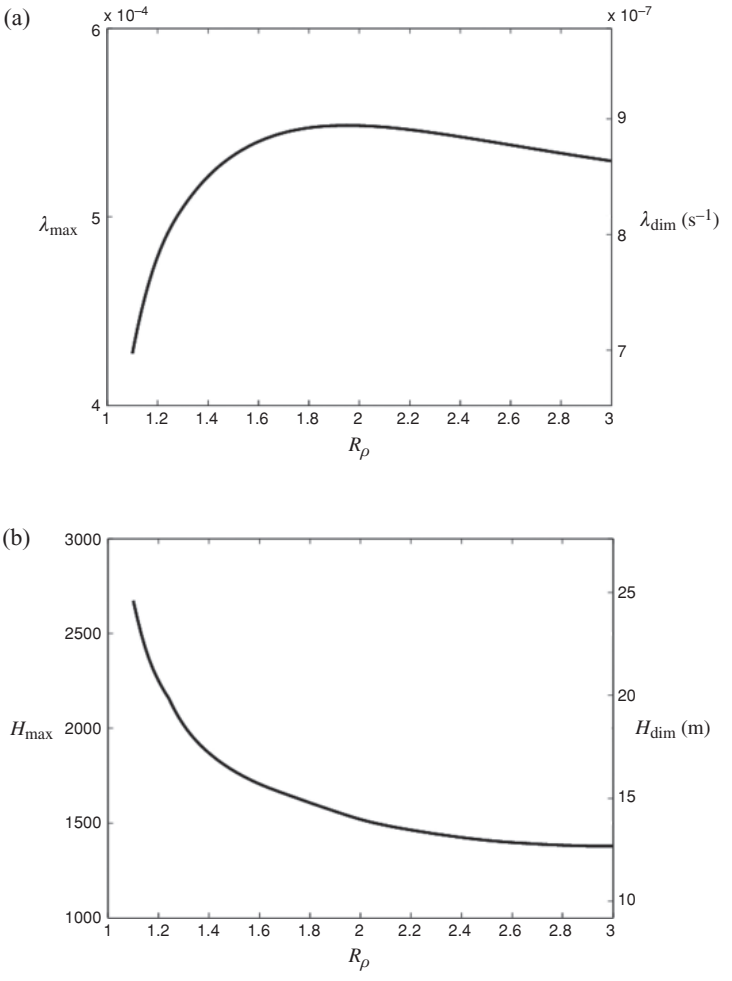

Figure 7.7 The maximal growth rate (a) and the corresponding thickness (b) of intrusions. The non-dimensional variables are indicated on the left axis. The corresponding dimensional values are for $\bar{T}_z = 0.01$ °C m^{-1}.

remains as in Figure 7.3: warm and salty intrusions move upward whereas the cold and fresh ones sink. Another observable intrusion characteristic is the amplitude ratio $a_r = \frac{\hat{T}}{\hat{S}}$, which measures the amplitude of the thermal component of density perturbation in the intrusion relative to its haline component (Fig. 7.6b). It monotonically increases with density ratio from $a_r = 1.2$ at $R_\rho = 1.1$ to $a_r = 2.2$ at $R_\rho = 2.3$. The growth rate (Fig. 7.7a) is non-monotonic: for R_ρ increasing from unity, $\lambda_{\max}$ first increases (somewhat counterintuitively) and then starts to gradually decrease for $R_\rho > 2$. The preferred vertical scale (Fig. 7.7b) also decreases with R_ρ. The non-dimensional wavelengths and growth rates have been converted

into dimensional units using the standard double-diffusive non-dimensionalization system in (1.11). The dimensional values are also shown in Figure 7.7 (right axes) for $\bar{T}_z = 0.01\,^{\circ}\mathrm{C\,m^{-1}}$, which is representative of thermal stratification in the mid-latitude thermocline.

Overall, the predictions of the parametric model in Figures 7.6 and 7.7 are consistent with the nominal observationally inferred intrusion characteristics. The preferred intrusions slopes ($s \sim 10^{-3}$), vertical wavelengths ($H_{\max} \sim 10$ m) and amplitude ratio ($a_r \sim 2$) conform to expectations, at least in the order-of-magnitude sense. The agreement is encouraging, given the minimal nature of the model. More quantitative comparisons require the inclusion of additional ingredients, such as baroclinicity and ambient turbulence (discussed in Section 7.2). And even then, the application of the parametric model is far from straightforward.

Similarity argument

Interleaving is known to be particularly active in strong fronts, which prompts the question of how their linear characteristics depend on lateral gradients of temperature and salinity. Some dependencies can be inferred based on the structure of the governing equations, without performing detailed calculations. Merryfield (2000) noted that for small intrusion slopes – an assumption that is definitely satisfied in the ocean – the governing system (7.1) is invariant with respect to the transformation

$$\begin{aligned} &t \to C^{-1}t, (x, y) \to C^{-\frac{3}{2}}(x, y), z \to C^{-\frac{1}{2}}z, \\ &G \to CG, \\ &(T', S') \to C^{-\frac{1}{2}}(T', S'), \\ &(u', \mathrm{v}') \to C^{-\frac{1}{2}}(u', \mathrm{v}'), w' \to C^{-\frac{3}{2}}w'. \end{aligned} \tag{7.3}$$

So, for instance, if the horizontal temperature and salinity gradients were increased by a factor C, while the vertical gradients were kept constant, then the time scale of intrusion growth would decrease by the exactly the same factor. Furthermore, invariance (7.3) implies that the maximal growth rate of intrusions ($\lambda_{\max}$), the corresponding vertical wavenumber ($m_{\max}$) and slope ($s_{\max}$) are related to the slope of isotherms G as follows:

$$\begin{cases} \lambda_{\max} \propto G, \\ m_{\max} \propto \sqrt{G}, \\ s_{\max} \propto G. \end{cases} \tag{7.4}$$

This elegant similarity argument effectively reduces the number of governing parameters in the intrusion problem. Stability characteristics need to be evaluated for a single value of G and (7.4) immediately extends the analysis to arbitrary G's.

It should be borne in mind that this isomorphism formally pertains only to the initial linear stage of the intrusion growth. The similarity relations (7.3) are not expected to be accurate after the appearance of convective overturns, which are characterized by flux laws that are different from those assumed for salt-finger regions (6.2). On the other hand, if these relations were to hold at least approximately in the nonlinear regime, this would imply that the equilibrium lateral fluxes due to interleaving $\left(\overline{u'T'} \propto C^{-1}\right)$ actually decrease with increasing lateral gradients $\left(\bar{T}_x \propto C\right)$. Such unusual dynamics would constitute an interesting precedent of a radical departure from Fick's law of diffusion. Conundrums of this nature reflect the challenges involved in the development of physical models of lateral intrusion-induced mixing and need to be addressed in future studies of interleaving.

Multiscale model

Recent years have witnessed significant progress in the development of the parametric model. However, a number of theoretical predictions – such as the dependence of intrusion scales on stratification, precise conditions for their occurrence, and the relative strengths of temperature and salinity signatures – are yet to be reconciled with measurements and simulations. While the parametric theory remains unquestionably the most popular means for explaining and predicting intrusion characteristics, it is prudent to explore alternatives. The heavy reliance of most interleaving models on parameterizations of microstructure, a source of great uncertainty in itself, might prove to be the Achilles' heel of contemporary intrusion theory. These concerns motivate the development of approaches based directly on the original governing equations rather than on empirical flux-gradient laws.

One of the prospects for analytical progress is related to the disparity of the salt-finger (centimeters) and intrusion (tens of meters vertically) scales. Since salt fingers operate on a distinct narrow-band range of wavelengths, problems concerning their interaction with larger scales of motion could be, but very seldom are, couched in terms of multiscale asymptotic analysis (Bensoussan *et al*., 1978; Mei and Vernescu, 2010). A rare example of the application of multiscale methods in double-diffusion was presented by Holyer's (1981, 1985) collective instability

model, discussed in Chapter 6. An analogous calculation for the intrusion problem (Radko, 2011) is briefly described below.

The first step in the multiscale model is the choice of background pattern, representing individual salt fingers, which is taken here to be harmonic in x and z:

$$T_{\mathrm{bg}} = A_T \sin(k_f x) \sin(k_f r z), \tag{7.5}$$

where A_T is the amplitude of temperature variation in salt fingers, k_f is the horizontal wavenumber of the individual fingers and r is the aspect ratio. Similar patterns are also assumed for salinity and streamfunction and the dependent variables are separated into the background field of salt fingers $\left(T_{\mathrm{bg}}, S_{\mathrm{bg}}, \psi_{\mathrm{bg}}\right)$ and a weak perturbation $\left(T', S', \psi'\right)$. Our immediate goal is to examine the linear stability of the background pattern with respect to the intrusive long-wavelength perturbations. The linearization of the governing equations, taken for simplicity to be two-dimensional Navier–Stokes, about the basic state yields:

$$\begin{cases} \dfrac{\partial T'}{\partial t} + \dfrac{\partial \psi_{\mathrm{bg}}}{\partial x}\dfrac{\partial T'}{\partial z} + \dfrac{\partial \psi'}{\partial x}\dfrac{\partial T_{\mathrm{bg}}}{\partial z} - \dfrac{\partial \psi'}{\partial z}\dfrac{\partial T_{\mathrm{bg}}}{\partial x} - \dfrac{\partial \psi_{\mathrm{bg}}}{\partial z}\dfrac{\partial T'}{\partial x} - G\dfrac{\partial \psi'}{\partial z} + \dfrac{\partial \psi'}{\partial x} \\ \qquad = \nabla^2 T', \\ \dfrac{\partial S'}{\partial t} + \dfrac{\partial \psi_{\mathrm{bg}}}{\partial x}\dfrac{\partial S'}{\partial z} + \dfrac{\partial \psi'}{\partial x}\dfrac{\partial S_{\mathrm{bg}}}{\partial z} - \dfrac{\partial \psi'}{\partial z}\dfrac{\partial S_{\mathrm{bg}}}{\partial x} - \dfrac{\partial \psi_{\mathrm{bg}}}{\partial z}\dfrac{\partial S'}{\partial x} - G\dfrac{\partial \psi'}{\partial z} + \dfrac{1}{R_\rho}\dfrac{\partial \psi'}{\partial x} \\ \qquad = \tau \nabla^2 S', \\ \dfrac{\partial}{\partial t}\nabla^2\psi' + \dfrac{\partial \psi_{\mathrm{bg}}}{\partial x}\dfrac{\nabla^2\psi'}{\partial z} + \dfrac{\partial \psi'}{\partial x}\dfrac{\partial \nabla^2 \psi_{\mathrm{bg}}}{\partial z} - \dfrac{\partial \psi_{\mathrm{bg}}}{\partial z}\dfrac{\nabla^2\psi'}{\partial x} - \dfrac{\partial \psi'}{\partial z}\dfrac{\partial \nabla^2 \psi_{\mathrm{bg}}}{\partial x} \\ \qquad = Pr\left[\dfrac{\partial}{\partial x}(T' - S') + \nabla^4 \psi'\right]. \end{cases} \tag{7.6}$$

Next, we introduce new spatial (X, Z) and temporal (t_0) scales to describe the slow evolution of large-scale perturbations. The intrusion scales are connected to the primary (salt-finger) scales by assuming simple power laws of the form:

$$X = \varepsilon^a x,\ Z = \varepsilon^b z,\ t_0 = \varepsilon^c t, \tag{7.7}$$

where $\varepsilon \ll 1$ is a small parameter. The reason for rescaling independent variables using a single expansion parameter (ε) is a pragmatic one. The singular perturbations theory is rigorously and systematically developed only for one asymptotic parameter, and multi-parameter problems have to be solved on a case-by-case basis (Kevorkian and Cole, 1996). The most common approach requires users to focus on specific sectors in the parameter space, selected on a physical basis. For the intrusion problem, an appropriate scaling (Radko, 2011), which ensures that

the model captures all essential dynamics, is given by $a = 3$, $b = 2$ and $c = 2$ in (7.7). The horizontal temperature gradient (G), another small parameter in the problem, is rescaled as $G = \varepsilon^3 G_0$. The subsequent development follows the conventional technique used in multiscale problems (e.g., Kevorkian and Cole, 1996; Mei and Vernescu, 2010): (i) (x, z, X, Z, t_0) are treated as independent variables; (ii) on short scales (x, z) we impose the same periodicity as in the basic flow; and (iii) derivatives in the governing system are replaced as follows:

$$\frac{\partial}{\partial x} \to \frac{\partial}{\partial x} + \varepsilon^3 \frac{\partial}{\partial X}, \frac{\partial}{\partial z} \to \frac{\partial}{\partial z} + \varepsilon^2 \frac{\partial}{\partial Z}, \frac{\partial}{\partial t} \to \varepsilon^2 \frac{\partial}{\partial t_0}. \tag{7.8}$$

The solution for $\left(T', S', \psi'\right)$ is obtained in terms of a series in ε:

$$\left(T', S', \psi'\right) = (T_0, S_0, \psi_0) + \varepsilon\,(T_1, S_1, \psi_1) + \varepsilon^2\,(T_2, S_2, \psi_2) + \cdots. \tag{7.9}$$

Equations (7.8) and (7.9) are substituted in (7.6) and terms of the same order in ε are collected. The resulting hierarchy of equations is sequentially solved until a closed, explicit solution is found that represents the evolution of the intrusive perturbation on large spatial and temporal scales. Stability of the modulational large-scale equations is analyzed using the normal modes proportional to $\exp(\lambda_0 t_0 + iKX + iMZ)$. The resulting growth rate equation can be expressed in terms of the original, rather than rescaled, variables. It takes the form of a fourth-order polynomial:

$$\lambda^4 + a_3\lambda^3 + a_2\lambda^2 + a_1\lambda + a_0 = 0, \tag{7.10}$$

whose coefficients a_i depend on $\left(A_T, m, \tau, R_\rho, Pr, G, s, r\right)$.

Predictions of the multiscale model (Figs. 7.8 and 7.9) are consistent with physical expectations and generally conform to the parametric model. Intrusions are oriented as in Figure 7.3 – with warm and salty (cold and fresh) water rising (sinking) across density interfaces. Typical growth rates are of the order $\lambda \sim 10^{-3}$, which corresponds to the dimensional time scale of days, and maximal intrusion slopes are of the order $s \sim 10^{-3}$.

A generic drawback of multiscale models is that the background pattern has to be specified a priori. In the intrusion problem, this implies knowledge of the amplitude of salt fingers (A_T) and their wavenumbers $\left(k_f, rk_f\right)$ in (7.5). While the horizontal wavenumber k_f can be adequately estimated on the basis of the linear model (Schmitt, 1979a), a simple theoretical prescription for the finger amplitude and the vertical wavenumber (or equivalently, the aspect ratio r) is still lacking. Nevertheless, this information is direct and often accessible in field measurements, in contrast to the flux-gradient laws used by the parametric model. Direct numerical simulations indicate that the amplitude depends on the density ratio and it is limited

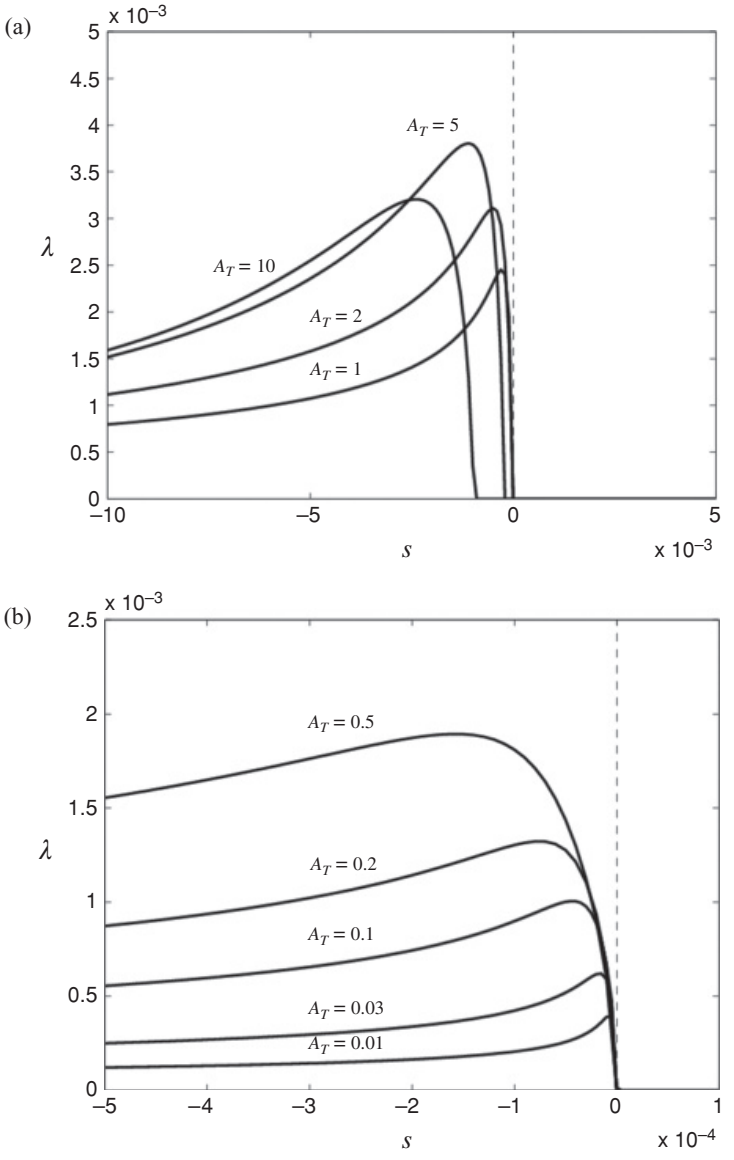

Figure 7.8 Multiscale model of interleaving. The maximal growth rate of intrusions is plotted as a function of slope (s) for various values of the salt finger amplitude (A_T) and a fixed value of finger aspect ratio ($r = 0.1$).

to the range $1 < A_T < 10$. The aspect ratio of salt fingers r is less than unity but, typically, is an order-one quantity (e.g., Taylor, 1993). The growth rates are sensitive to both A_T (Fig. 7.8) and r (Fig. 7.9), but the overall pattern of the $\lambda(k, m)$ relation appears to be structurally robust.

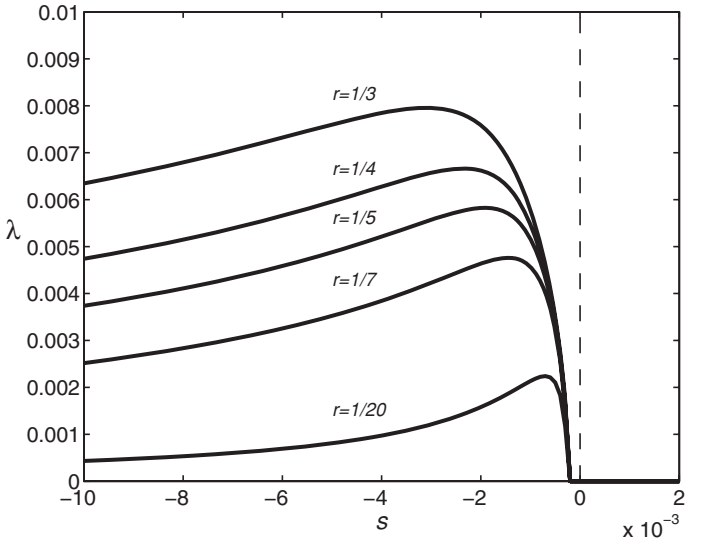

Figure 7.9 Multiscale model of interleaving. The maximal growth rate of intrusions is plotted as a function of slope (s) for various values of the finger aspect ratio (r) and a fixed value of the salt finger amplitude ($A_T = 5$).

A significant advantage of the multiscale approach, as compared to parametric modeling, is related to its transparency and, perhaps, deeper insight into the dynamics at play. The multiscale model shows explicitly how various Fourier harmonics of individual salt fingers are affected by the large-scale advection and how these finger modes constructively interact to provide a positive feedback on the intrusion. Parameterized models lose all of the connection with the dynamics of individual fingers immediately after assuming an expression for fluxes. This connection is retained by multiscale models from the first step to the last. While multiscale modeling for double-diffusion is still in a preliminary exploratory stage, its potential for addressing scale interaction problems in double-diffusion is already evident (Holyer, 1981, 1985; Radko, 2011). It is perhaps ironic that multiscale techniques have been used more frequently in configurations (Cushman-Roisin *et al*., 1984; Gama *et al*., 1994; Manfroi and Young, 1999; among many others) where the scale separation is not nearly as well-defined or physically justified as in the salt-finger problem.

7.2 Extensions: rotation, baroclinicity and ambient turbulence

Having examined in considerable detail the simplest configuration (Section 7.1), we now consider some oceanographically relevant extensions.

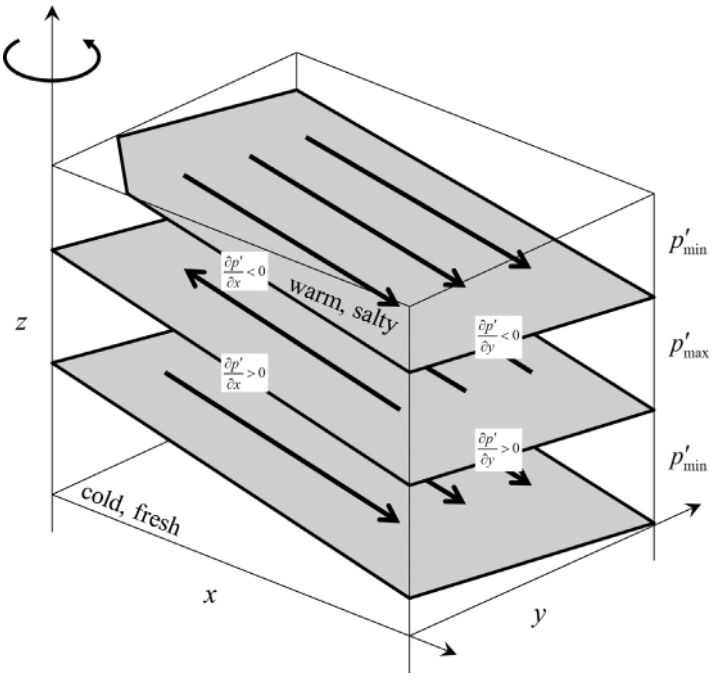

Figure 7.10 Schematic diagram illustrating the effects of rotation on finger-driven intrusions. The fastest growing intrusion develops a finite along-front slope.

Rotation

Given their slow evolutionary time scales (days), it seems likely that intrusions could be affected by planetary rotation. In reality, rotational effects in the barotropic model are rather modest. By and large, rotation does not affect the growth rate, height and the cross-front slope of the fastest growing intrusions. The most notable observable consequence of rotation is the development of a systematic tilt of intrusions in the along-front direction, as indicated in the schematic in Figure 7.10.

In order to physically interpret the rotational along-front tilt, let us have a brief look back at Figure 7.3, illustrating the essence of the intrusion mechanics, and modify this scenario by adding rotation. Planetary rotation affects circulation primarily by means of the Coriolis force. To be specific, consider dynamics realized in the Northern Hemisphere, where the Coriolis force is directed to the right of the fluid motion. Thus, intrusions advecting fluid upward (downward) in the x–z plane are forced in the positive (negative) y-direction by the Coriolis force. The next step is readjustment of the pressure distribution, which tends to balance the Coriolis force and thereby maintain the geostrophic equilibrium. A detailed calculation indicates that intrusions are fully adjusted (e.g., McDougall, 1985a) – the pressure

gradient force exactly balances the Coriolis force and the along-front velocity is zero. In order to balance the Coriolis force, the along-front gradient should be positive $\left(\frac{\partial p'}{\partial y} > 0\right)$ in the upward moving intrusions and negative $\left(\frac{\partial p'}{\partial y} < 0\right)$ in the downward. How does the induced pressure distribution affect the intrusion growth? Consider first intrusions oriented as in Figure 7.10 – slightly sloping downward in the y-direction. In this case, the maximal values of the perturbation pressure are attained below the downward-moving intrusions and above the upward-moving ones. In terms of pressure distribution at the cross-front (x,z) section, this implies that in the upward-moving intrusions $\frac{\partial p'}{\partial x} > 0$. Thus, the rotationally induced pressure gradients reinforce the initial tendency: upward intrusions, moving towards the fresher side of the front, are further accelerated in the same direction. Similarly, downward intrusions are accelerated in the positive x-direction by the induced pressure gradient force. As a result, the along-front tilt in Figure 7.10 promotes the intrusion growth. On the other hand, if intrusions were tilted along the front in the opposite sense (sloping upward in y) the induced pressure gradients would act to suppress their growth. Hence, the configuration in Figure 7.10 represents the preferred orientation of intrusions, which is expected to be realized in nature as long as the selective advantage of the most rapidly growing modes is sufficient to ensure their dominance.

The analysis of intrusions driven by molecular fluxes (Kerr and Holyer, 1986) has led to similar conclusions: rotation tilts intrusions in the along-front direction but has little to no effect on other observable intrusion characteristics. Most theoretical intrusion models are concerned with the prediction of growth rates and vertical scales – quantities that control the intensity of lateral intrusion-driven mixing. Therefore, in the barotropic configuration, rotation is usually ignored for reasons of tractability. Effects of rotation, however, become more profound in the context of the baroclinic interleaving problem, which we consider next.

Baroclinicity

So far, our discussion has been focused on barotropic fronts with horizontally uniform background density. In most cases, however, horizontal density variation across oceanic fronts is significant, motivating "baroclinic" models, which take horizontal density stratification into account. Baroclinicity affects intrusions in two major ways (May and Kelley, 1997). First, there is a set of consequences directly related to the geometry of the system. The horizontal density stratification projects on the density variation along the intrusion itself, which can either intensify interleaving or suppress it. Various configurations are illustrated in Figure 7.11. When isohalines and isopycnals are inclined in the opposite sense (Fig. 7.11b), the

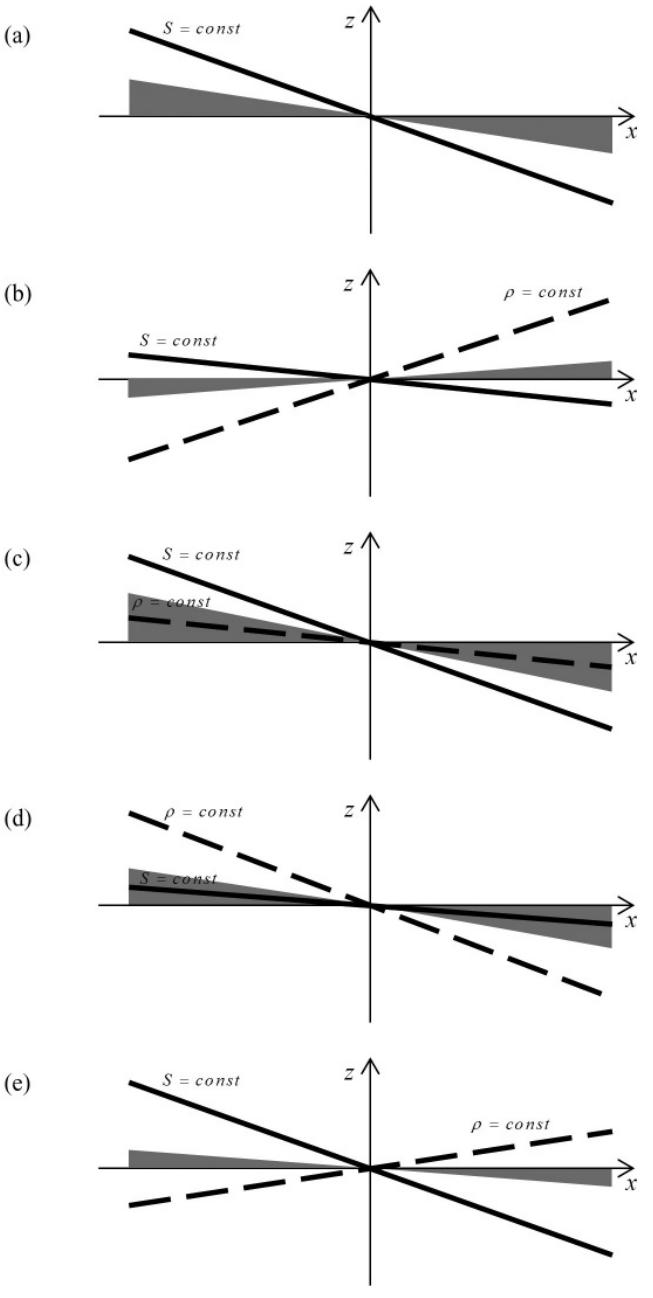

Figure 7.11 The effects of baroclinicity on finger-driven intrusions. Shading indicates the range of slopes susceptible to interleaving for various orientations of isohalines and isopycnals in (a)–(e).

density gradient along the intrusion increases relative to that in the barotropic case (Fig. 7.11a). The increase in stratification adversely affects the ability of intrusions to advect fluid across the isopycnals. As a result, intrusion growth rates decrease and the range of slopes for which unstable solutions exist reduces. On the other hand, if isohaline and isopycnal slopes are of the same sign (Fig. 7.11c), the density gradient along the intrusion is reduced. With the stabilizing influence of density stratification diminished, intrusions are able to accelerate faster and instability affects a wider range of slopes. Very different dynamics are realized when the isopycnals are inclined more steeply than isohalines (Fig. 7.11d,e). In this case, the instability region extends beyond the haline wedge $\left(-S_x/S_z < s < 0\right)$, outside of which double-diffusive effects become secondary and the dynamics become similar to the classical baroclinic instability. Predominantly baroclinic instabilities, however, are characterized by much larger vertical scales and therefore their connection with the observed ($\sim$10 m) intrusions is questionable.

The second set of baroclinic effects is associated with vertical shear. The geostrophic along-front velocity is directly linked to the cross-front density gradient by the thermal wind balance:

$$f\bar{\mathrm{v}}_{z\,\mathrm{dim}} = -\frac{g}{\rho_0}\bar{\rho}_{x\,\mathrm{dim}}, \tag{7.11}$$

and therefore vertical shear is omnipresent at baroclinic fronts. Unlike the geometric effects (Fig. 7.11), which could enhance or suppress intrusions, shear consistently acts against intrusion growth. One such mechanism is based on the suppression of the along-flow variation in temperature and salinity by shear. Since the fastest growing intrusion modes are characterized by a finite along-front slope (Fig. 7.10) – hence significant along-front *T*/*S* variation – the tendency of shear to homogenize the flow in this direction inevitably reduces the maximal growth rate. When shear is realistically strong, the relevant fastest growing modes represent the pure cross-flow intrusions with $l \approx 0$ (e.g., Smyth, 2008). Other adverse shear-induced effects include (i) a reduction in the intensity of salt fingering caused by the tilting of fingers in the direction of shear and (ii) an enhanced probability of turbulent overturns in the high-shear environment. Both processes modify vertical diffusivities of temperature and salinity, making double-diffusion less effective in driving intrusions.

To the best of our knowledge, it has not been determined which set of baroclinic processes, geometric or shear-induced, is more significant for intrusion dynamics. The answer is likely to depend on a particular problem and background parameters – baroclinicity, stratification, and the level of ambient turbulence. It should be noted that *horizontal* shear also tends to inhibit thermohaline interleaving (Worthem *et al*., 1983) through mechanisms that are similar to those at work in

vertical (baroclinic) shear. The horizontal along-front shear homogenizes the flow in the downstream direction and thereby suppresses the fastest growing modes, which, in the presence of rotation, have a finite along-front slope.

Ambient turbulence

Within the stratified interior of the ocean, small-scale vertical mixing is accomplished by a combination of double-diffusion and mechanically generated turbulence, usually associated with overturning gravity waves (e.g., Gregg, 1987; Gargett, 1989; Thorpe, 2005). Generally, small-scale turbulence is thought to be ineffective in driving intrusions. It was shown by Stern (1967) and is apparent from the physical interpretation (Fig. 7.3) that unequal eddy diffusivities of heat and salt are essential for the spontaneous generation of interleaving motions. Fully developed turbulence, on the other hand, tends to mix temperature and salinity at equal rates. An exception is provided by differential diffusion – an incomplete turbulent mixing by weak turbulence in a strongly stratified environment. Differential diffusion is characterized by higher diffusivity of temperature and therefore it has been invoked to explain the appearance of intrusions in double-diffusively stable regions (Hebert, 1999; Gargett, 2003; Merryfield, 2002). However, the existing evidence for its general importance is, at present, too circumstantial to warrant a detailed analysis.

We proceed under a conventional assumption that eddy diffusivities of heat and salt due to mechanical turbulence are nearly equal ($K_{\rm turb}$) but can differ from the turbulent eddy viscosity ($A_{\rm turb}$). Another common, albeit less justified, approximation represents the net small-scale mixing as a sum of the contribution from double-diffusion and turbulence:

$$\begin{cases} K_T = K_{T\,\rm dd} + K_{\rm turb}, \\ K_S = K_{S\,\rm dd} + K_{\rm turb}, \\ K_M = K_{M\rm dd} + A_{\rm turb}, \end{cases} \tag{7.12}$$

where (K_T, K_S, K_M) are the diffusivities of temperature, salinity and momentum respectively. Subscripts dd (turb) denote the contribution from double-diffusion (turbulence). The general structure of (7.12) suggests that the impact of turbulence on interleaving is two-fold. Taking turbulence into account (i) effectively increases the net viscosity and (ii) brings the ratio of eddy diffusivities of heat and salt closer to unity. At first, it appears that both effects should have an adverse effect on interleaving. The reality, however, is not as clear-cut – the devil is in the details.

Consider first viscous effects. Double-diffusion by itself is a highly ineffective mixer of momentum. Eddy viscosity due to salt fingers is much less than

the diffusivity of heat or salt; it is even less than molecular viscosity. Therefore, the presence of even a very modest amount of ambient turbulence, typical of the main thermocline, can dramatically increase the net viscosity (K_M) leaving the *T–S* diffusivities largely unchanged. Viscous damping tends to selectively suppress relatively small-scale features – the larger the viscosity, the wider is the range of scales affected by it. In this way, viscosity can exert a controlling influence on the vertical scale of intrusions. An increase in viscosity systematically shifts the range of vertical wavelengths affected by interleaving instability towards longer scales. Since intrusion models based on molecular viscosity (Fig. 7.7b) predict relatively modest vertical scales ($H_{\mathrm{dim}} \sim$ 10–20 m) the presence of much larger intrusions in the ocean ($\sim$100 m) can be plausibly attributed to turbulent mixing. The major difficulty with this argument, of course, is that vertical eddy viscosity in the ocean is poorly constrained and spatially variable, which precludes its unequivocal corroboration. It should also be kept in mind that effects of turbulence on intrusions could be very different at barotropic and at baroclinic fronts. Turbulence can suppress interleaving entirely for strongly baroclinic conditions (Kuzmina and Zhurbas, 2000; Zhurbas and Oh, 2001), whereas in the barotropic model interleaving persists regardless of the strength of ambient turbulence, albeit intrusion growth rates are reduced (Walsh and Ruddick, 2000).

For historical reasons, it is interesting to note that the first intrusion model (Stern, 1967) did not take viscosity, molecular or eddy-induced, into account. As a result, the preferred vertical scale was absent in Stern's (1967) formulation. The growth rate of intrusive instabilities monotonically increased with decreasing height. The source of this problem was identified by Toole and Georgi (1981). They noted that the inclusion of vertical momentum flux removes the ultraviolet catastrophe in Stern's model and makes it possible to estimate the basic characteristics of intrusions by focusing on the fastest growing mode.

While the damping tendency of friction is intuitive and predictable, the possibility for viscous destabilization is anything but. Nevertheless, such a possibility is very real for interleaving motions. It was noted by McIntyre (1970) that a distinct class of instabilities can be induced by differences in eddy viscosity and diffusivity. If the eddy Prandtl number $\left(Pr_e = \frac{K_M}{K_T}\right)$ exceeds unity, the baroclinic flow becomes susceptible to instabilities that are similar to the classical thermohaline intrusions in pattern but dynamically different. Also characterized by vertically periodic structure and inclined at small angles, McIntyre modes are not dependent on unequal diffusivities of heat and salt.

The essence of the McIntyre effect resides in the ability of elevated friction to upset the equilibrium balances of stable frictionless motions. Consider for instance the configuration in Figure 7.12. Displacements within the baroclinic instability

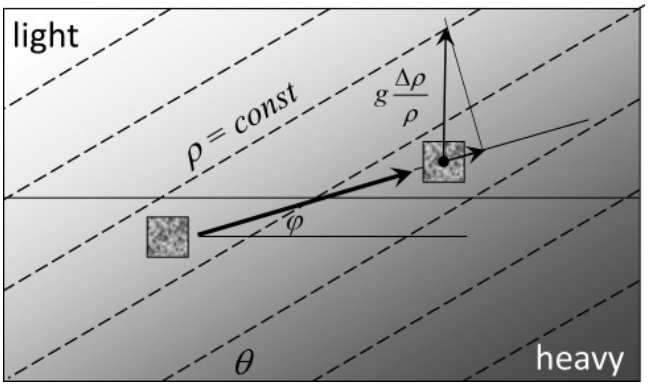

Figure 7.12 Schematic diagram of the McIntyre instability. In the baroclinic model, displacement of a fluid element upward within the wedge of instability places it in denser surroundings. The resulting upward buoyancy force tends to reinforce the initial displacement, thereby supporting the instability.

wedge ($0 < \varphi < \theta$) bring lighter fluid upward. This, by itself, suggests instability: the upward buoyancy force reinforces the initial perturbation. However, in the ideal (frictionless, non-diffusive) fluid, this tendency is countered by the Coriolis force, which consistently acts to the right – we are still in the Northern Hemisphere – and ultimately reverses the direction of the initial displacement. The result is a stable periodic oscillation known as the inertia-gravity wave. Now, let us reintroduce viscosity, high enough to dramatically reduce the perturbation velocity. The density perturbation, we assume, remains of the same magnitude as before. In this regime, the Coriolis effect is reduced to such low levels that it is no longer able to counteract the destabilizing buoyancy forcing. The perturbation monotonically grows in time.

The McIntyre instability operates at the intermediate range of vertical scales ($\sim$10–100 m), which makes it difficult to distinguish it from thermohaline intrusions on the basis of oceanographic observations. The situation is further complicated by the very likely possibility that both effects are simultaneously present and interact in a non-trivial manner. The ocean is at least triply diffusive. The rates of heat, salt and momentum dissipation are unequal. Their relative significance varies in space and time, and so do intrusion properties. For instance, Ruddick (1992) analyzed intrusions operating on the lower flank of meddy Sharon and established their predominantly thermohaline origin. Intrusions operating on the Faroe Front – another well-studied (Hallock, 1985) example of interleaving – are better described by the McIntyre model.

Smyth and Ruddick (2010) systematically analyzed the linear parametric intrusion model in terms of its sensitivity to the level of ambient turbulence. The key

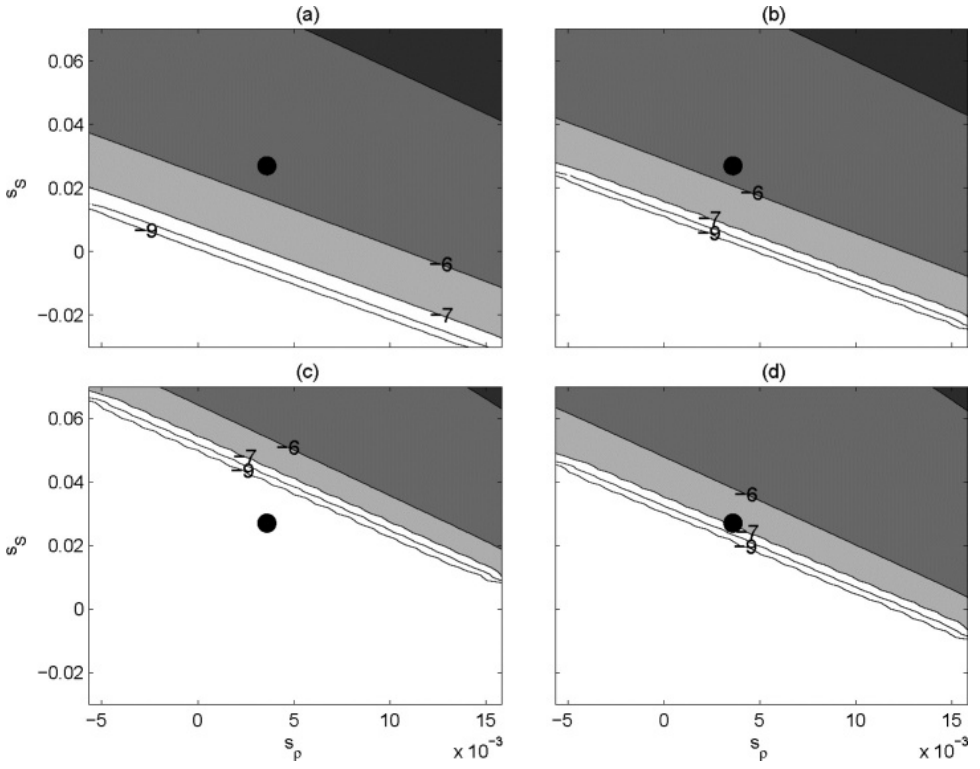

Figure 7.13 Common logarithm of the growth rate of the fastest growing interleaving mode as a function of isohaline and isopycnal slopes (darker shading corresponds to larger growth rates). Diffusivities are (a) double-diffusive only; (b) double-diffusive and molecular; (c) double-diffusive, molecular and turbulent with $Pr_e = 1$; and (d) same as (c) except $Pr_e = 20$. Large filled circles indicate the isopycnal and isohaline slopes characteristic of the lower flank of meddy Sharon. From Smyth and Ruddick (2010).

results are summarized in Figure 7.13. Adding turbulent mixing with the turbulent Prandtl number of unity to the double-diffusive model substantially reduces growth rates and shrinks the unstable region in the (s_S, s_ρ) parameter space. This effect is partially reversed when the Prandtl number is increased significantly above unity (Fig. 7.13d), which apparently reflects McIntyre dynamics at play. An increase in turbulent diffusivity (K_{turb}) generally tends to stabilize the system. Figure 7.14a shows the uniform retreat of the intrusion-favorable region following an increase in $\mu = \frac{K_{\text{turb}}}{K_{S\,\text{dd}}}$. The exception (of course there is an exception – it is double-diffusion!) is the strongly turbulent regime in which $\mu \gg 1$. In this case, the dynamics become essentially McIntyre-driven and the instability is determined by the orientation of isopycnals; the isohaline slope is largely irrelevant. The result is the tilting of the stability boundary in the (s_S, s_ρ) space towards the line $s_\rho = const$ with increasing μ

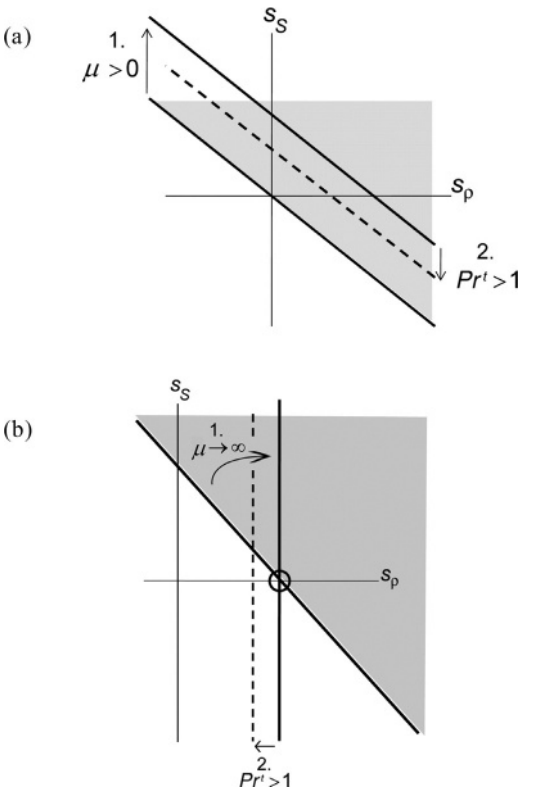

Figure 7.14 (a) Schematic showing the lowest-order effects on the stability boundary due to the imposition of weak turbulent thermal diffusivity (arrow 1) and an increase in the turbulent Prandtl number (arrow 2). Shading indicates instability. (b) Schematic for the "strong turbulence" limit, showing the tilting of the stability boundary as $\mu \to \infty$ (arrow 1) and the expansion of the unstable region as the turbulent Prandtl number is increased above unity (arrow 2). From Smyth and Ruddick (2010).

(Fig. 7.14b). This change is stabilizing if the slopes of isohalines and isopycnals are of the same sign. If not, the increase in turbulent diffusivity destabilizes the system.

7.3 Nonlinear effects

As suggestive and interesting as linear theories are, they are severely limited by (i) their principal inability to predict the amplitude of fully developed intrusions and (ii) an uncertainty in the relevance of inferred characteristics for the nonlinear stage. Problems with nonlinear analysis are exacerbated by the tendency of intrusions to transform profoundly during their evolution. This tendency is related to the subcritical nature of intrusive instabilities.

With respect to nonlinear effects, most instabilities can be separated into two distinct categories. Instabilities where nonlinearity tends to suppress linear growth are known as supercritical. Unstable supercritical modes can equilibrate at relatively low amplitudes. In subcritical instabilities, on the other hand, nonlinearity reinforces the linear growth and therefore their equilibration generally occurs after the system evolves into a new state, dynamically different from the original configuration. Secondary large-scale double-diffusive instabilities generally tend to be subcritical and intrusive instabilities are no exception. The existing evidence – laboratory, observational and numerical – is consistent with the subcritical character of interleaving. The growth of salt-finger intrusions usually persists until they develop inversions in the T–S profiles, where salt fingering is partially supplanted by diffusive and convective mixing.

In such circumstances, standard analytical techniques of weakly nonlinear theory, which builds upon linear results, are of limited use. Only a few analytical results have been reported for fully nonlinear intrusions. McDougall (1985b) formulated a set of necessary conditions for the existence of steady-state solutions. Intrusions in his model were represented by a series of vertically homogeneous mixed layers separated by thin high-gradient interfaces with alternating diffusive and salt-finger favorable stratification. Tractability was achieved by assuming that the T–S fluxes are determined by the salinity variation across the interfaces rather than by local gradients. Kerr (1992, 2000) examined secondary instabilities of finite amplitude intrusions, albeit molecularly driven, and concluded that the equilibrium states are unstable with respect to secondary two- and three-dimensional perturbations – an important suggestion offering a first glimpse into the complexity of the equilibrium intrusion dynamics.

In view of the difficulties inherent in the analytical modeling of nonlinear intrusions, more promising (and definitely more popular) are models based primarily on numerical methods. Let us review a couple of the most common categories. First, there is the class of one-dimensional intrusion models, which extend the parametric theory (Section 7.1) into the nonlinear regime (Walsh and Ruddick, 1998; Merryfield, 2000; Mueller *et al.*, 2007). Such models assume that large-scale properties of intrusions are uniform along the intrusion fronts and therefore

$$T = T(\eta, t), \tag{7.13}$$

where the variable η represents the coordinate normal to the intrusion fronts; analogous expressions are assumed for S and ψ. For such patterns, the advective terms in the governing Navier–Stokes equations vanish identically. Nonlinearities now appear only in the expressions for fluxes (F_T, F_S) in (7.1). The parameterization

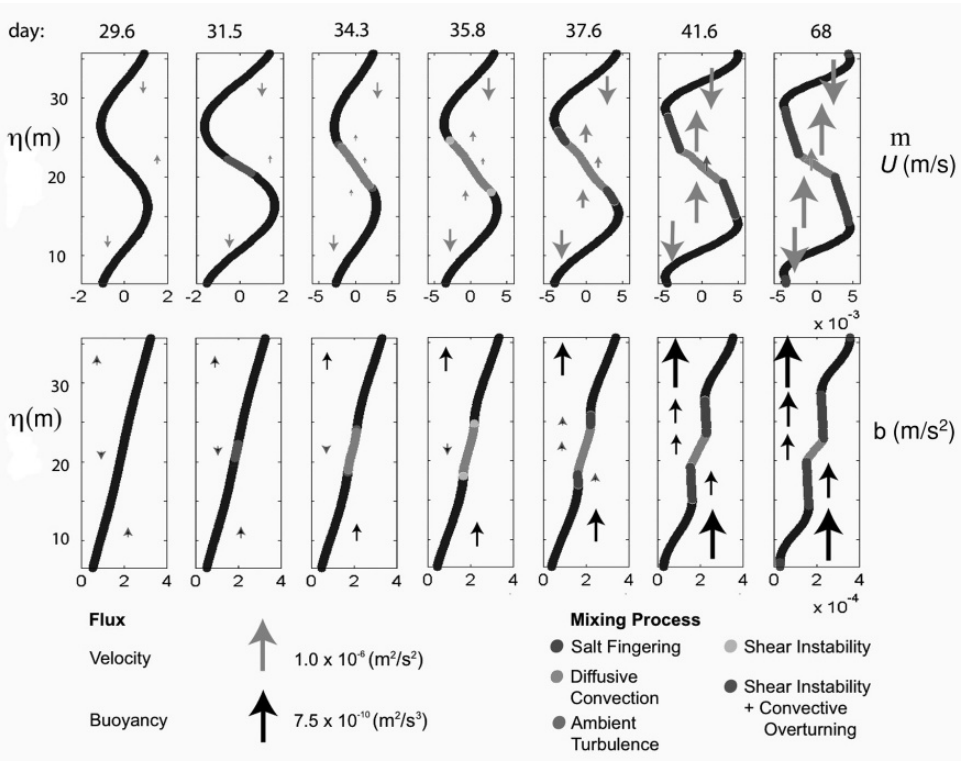

Figure 7.15 Evolution of velocity (top panel) and buoyancy (bottom panel) profiles. Arrows indicate across-intrusion fluxes. From Mueller *et al*. (2007).

of mixing necessarily involves assuming distinct flux-gradient laws for regions controlled by salt fingering, diffusive convection and convective or shear-driven turbulence.

The apparent advantage of one-dimensional models lies in their efficiency. After substitution of (7.13) and the corresponding expressions for S and ψ in the governing equations, the problem reduces to integration of a system of partial differential equations in (η, t). The simplicity of such models makes it possible to explore the parameter space in considerable detail, something that is still computationally prohibitive for direct numerical simulations (DNS). Figure 7.15 represents a typical evolution of the buoyancy field in the one-dimensional parametric model. This calculation (Mueller *et al*., 2007) was initiated by a small-amplitude harmonic perturbation; the slope and the vertical scale were chosen in a way that maximizes the linear growth rate. In time, the system evolved into a layered configuration consisting of alternating diffusive and salt-finger interfaces separated by well-mixed layers – the "conventional" intrusion pattern. As was pointed out by Merryfield (2000), other scenarios are also possible, including

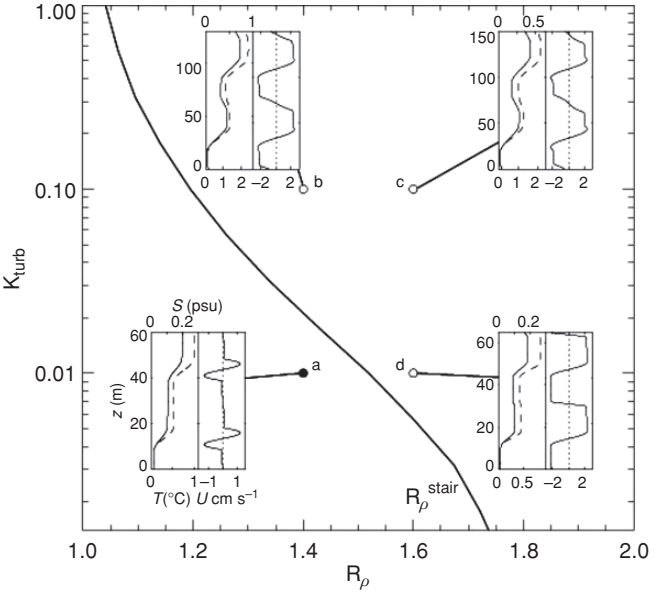

Figure 7.16 Equilibria of intrusions as a function of the density ratio (R_ρ) and turbulent diffusivity (K_{turb}). Insets show profiles of S (solid curves in the left panels), T (dashed curves), and horizontal velocity u for equilibrated intrusions as functions of z. The heavy solid curve separates the low-R_ρ region characterized by staircase patterns from the high-R_ρ region of conventional intrusions (see the inserts). From Merryfield (2000).

the "staircase" configuration characterized by the absence of diffusive interfaces. This regime is realized for relatively low density ratios. Figure 7.16 attempts to map the regions occupied by conventional intrusions and staircase solutions in the $\left(R_\rho, K_{\text{turb}}\right)$ parameter space. While the parametric model can be extended to two and three dimensions, attempts of this nature are rather rare. Merryfield (2000) reports two-dimensional parametric simulations of intrusions which, for computational reasons, have not been carried on into the strongly nonlinear regime characterized by vigorous density overturns. However, no fundamental obstacles exist for multi-dimensional parametric simulations of fully nonlinear interleaving. On the contrary, the successful implementation of three-dimensional parametric modeling for the collective instability problem (Radko and Stern, 2011) suggests that such simulations can and should be profitably explored for interleaving studies as well.

While the significance of the conceptual insights generated by one-dimensional parametric models is apparent, their ability to produce accurate quantitative predictions is questionable. The limitations of one-dimensional models include (i) their reliance on mixing parameterizations, (ii) their inability to represent the

along-intrusion variation of properties and (iii) the a-priori prescription of the intrusion slope (s). At this point I can imagine a frustrated reader complaining, "Why won't they just use DNS? Let's stop the guesswork and produce something reliable!" It is not that easy. Despite the rapid advancement of computational capabilities, the challenge of modeling salt-finger driven intrusions directly, without invoking various simplifying assumptions, has not been met. The fundamental problem is associated with their small slopes, which are typically on the order of $s \sim 10^{-3}$. The vertical scale of intrusions ($\sim$10 m) does not present a major computational problem in itself, but the associated horizontal scale $L_x \sim H/s \sim 10\,\mathrm{km}$ does. The requirement to simultaneously resolve salt fingers ($\sim$1 cm) and horizontal intrusions wavelengths ($\sim$10 km) is beyond the capabilities of even the most advanced super-computers.

Fortunately, the problem of scale disparity in the intrusion problem can be, to some extent, bypassed using the "tilted DNS" model. In what appears to be a very sensible compromise between realism and convenience, Simeonov and Stern (2007) proposed integrating the governing equations in the tilted coordinate system (ξ, η) aligned along the intrusion fronts (see the schematic in Fig. 7.17a). Doubly periodic boundary conditions are assumed for the perturbation fields in ξ and η. The tilted DNS configuration makes it possible to simulate intrusions of arbitrary slope using a modest computational domain ($L_\xi \sim L_\eta$). Of course, there is a price to pay: the intrusion slope throughout the simulation is given by the initially prescribed value. Thus, the possibility that the slope could change in time is a-priori excluded. On the positive side, mixing is now simulated explicitly and not parameterized. This advantage becomes critical in the fully nonlinear stages of simulation. The equilibrium state is characterized by complicated interactions between various components – large-scale shear, salt fingers, diffusive interface, convective turbulence. These interactions are very difficult, if not impossible, to accurately represent in the parametric model.

Figures 7.18–7.20 (Hebert, 2011) give us a glimpse into the remarkably rich phenomenology of interleaving. All experiments were performed using the tilted DNS model and initiated by a small amplitude harmonic (normal mode) perturbation in T, S and ψ. For each value of $\left(R_\rho, G\right)$, Hebert (2011) considered a range of vertical scales and slopes comparable with, but not necessarily identical to, the fastest growing values. The most common outcome of such experiments is the quasi-equilibrium state consisting of diffusive and salt-finger interfaces separated by a well-mixed convective zone (Fig. 7.18). The simulation in Figure 7.19 is different. As the intrusion grows, its along-front velocity reaches magnitudes sufficient to trigger secondary Kelvin–Helmholtz instability, manifested in the formation of mixing billows, which profoundly affect the flow pattern and its dynamics.

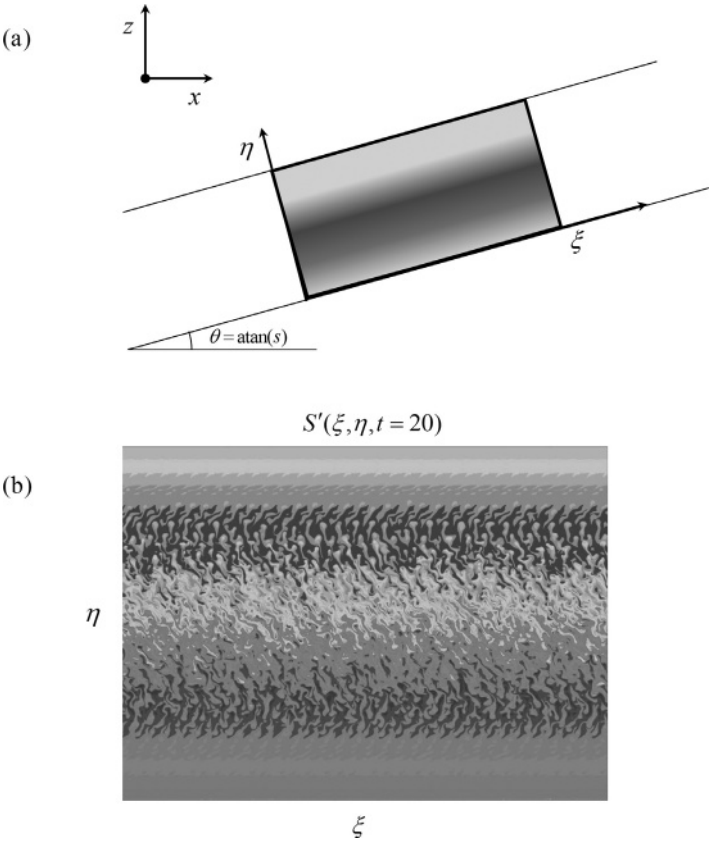

Figure 7.17 The "tilted box" modeling of intrusions. (a) Schematic diagram of the computational domain. The new coordinates are oriented along (ξ) and normal to the intrusion fronts (η). (b) Initial stage of linear intrusion growth in DNS. Presented is the departure of salinity from the background gradient. From Simeonov and Stern (2007).

The experiment in Figure 7.20 results in the staircase configuration, characterized by the absence of diffusive interfaces. Tilted DNS simulations reveal another effect that would have been impossible to identify with, and difficult to incorporate in, the one-dimensional models – the spontaneous generation of gravity waves. Figure 7.21 shows the evolution of the diffusive interface in time, the most pronounced feature of which is the cyclic amplification and breaking of waves, propagating along the intrusion fronts.

One of the evolutionary features of interleaving, which has not been fully explored by DNS, involves the sequential mergers of intrusions. Such mergers are often observed in laboratory experiments (Thorpe *et al*., 1969), in the solutions of the one-dimensional parametric model (Walsh and Ruddick, 1998) and in the

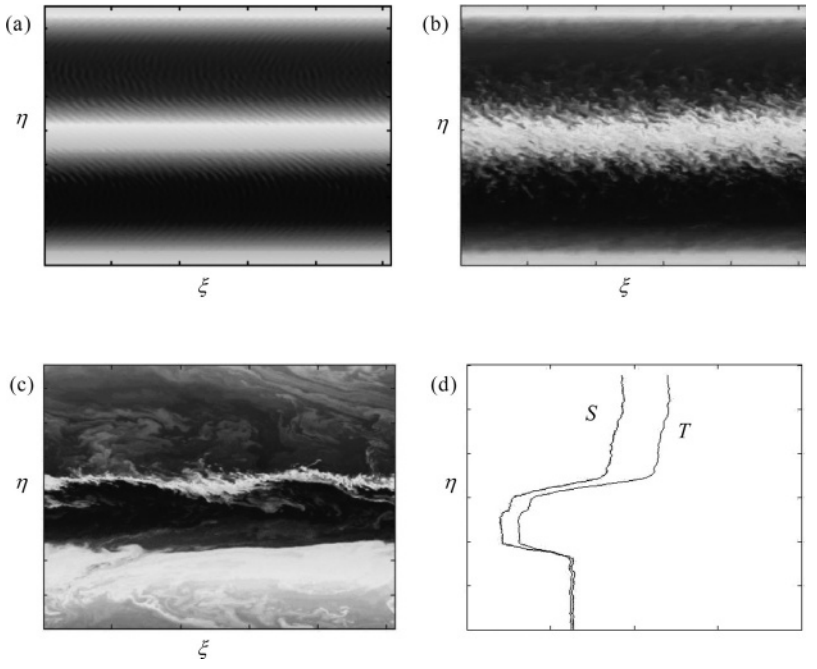

Figure 7.18 Growth and equilibration of "conventional" intrusions in the tilted DNS. (a)–(c) show the temperature perturbation at various stages of intrusion development. The vertical profiles of temperature and salinity in the final state are shown in (d). From Hebert (2011).

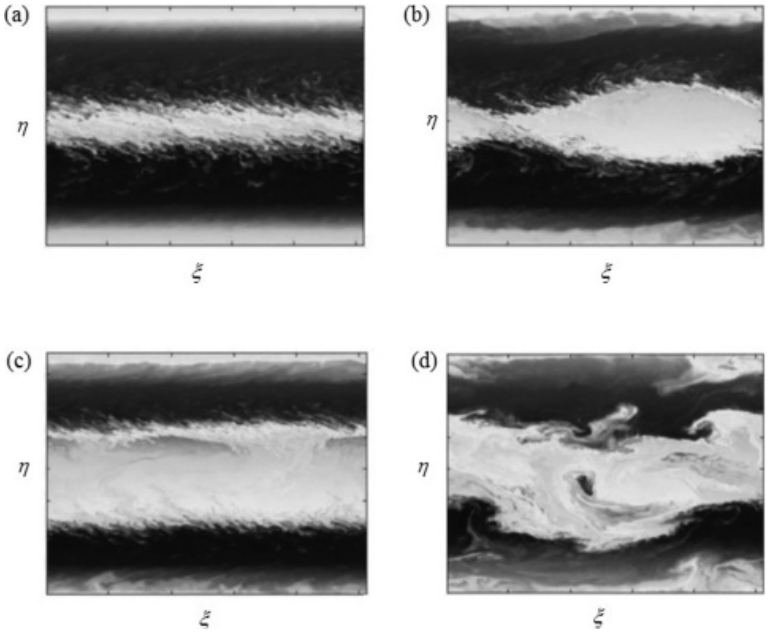

Figure 7.19 Growth and equilibration of intrusions susceptible to Kelvin–Helmholtz instabilities. The temperature perturbation is shown at various stages of intrusion development in (a)–(d). Red color corresponds to high values and low values are shown in blue. From Hebert (2011). See color plates section.

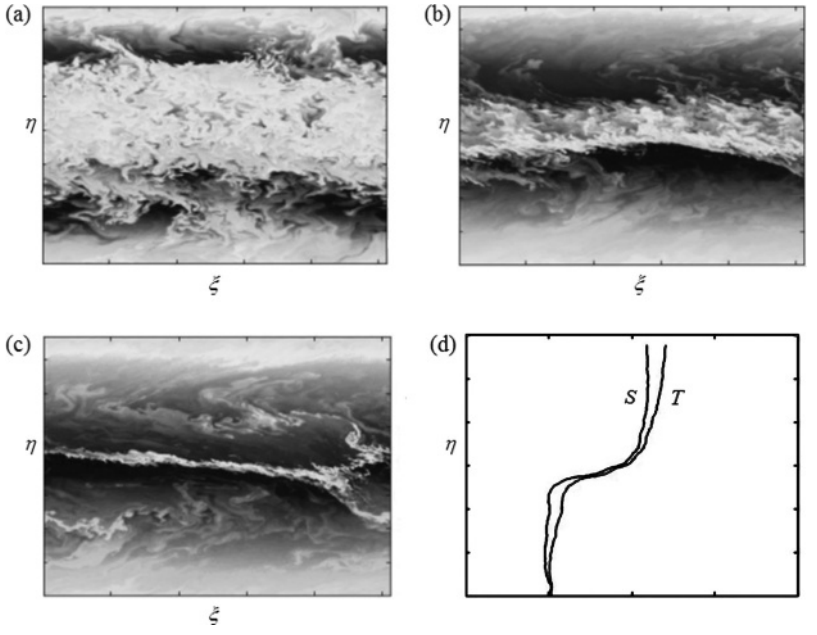

Figure 7.20 An experiment resulting in the staircase-type intrusion. The temperature perturbation is shown at various stages of intrusion development in (a)–(c). The vertical profiles of temperature and salinity in the final state are shown in (d). From Hebert (2011).

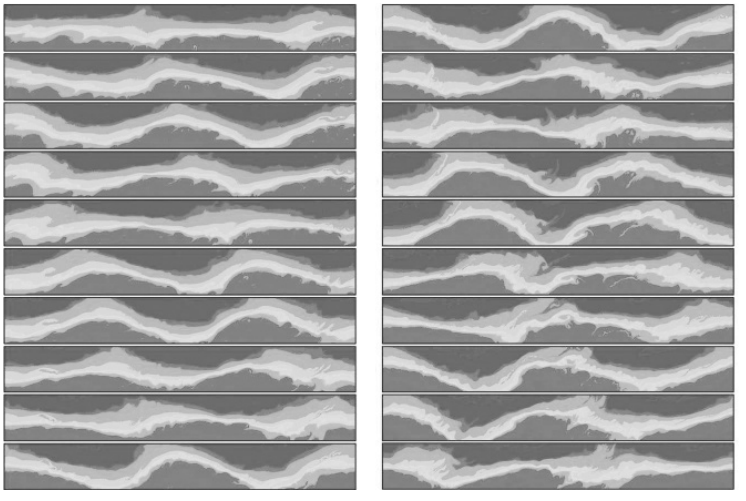

Figure 7.21 Generation of interfacial waves across the diffusive interface in the equilibrated intrusion (a tilted DNS experiment). Presented is the total salinity field in the immediate vicinity of the interface. Time is increasing downward along the left panels and then continues at the top right panel. From Simeonov and Stern (2007).

DNS of intrusions driven by molecular fluxes (Simeonov and Stern, 2008). Merging appears to be a generic property of double-diffusive structures, not limited to interleaving. For instance, layer-merging events are common in thermohaline staircases and play a prominent role in the establishment of a final quasi-equilibrium state (Huppert, 1971; Radko, 2005). For finger-driven intrusions in DNS, mergers have only been briefly mentioned by Simeonov and Stern (2007), although the merging phenomenon deserves further in-depth investigation. The significance of merging, should it prove to be ubiquitous in doubly diffusive fluids, lies in the appearance of structures with dimensions significantly exceeding the scale of the fastest growing modes. In this case, most predictions based on the linear theory have to be critically reevaluated.

An interesting question concerns the direction and magnitude of the net vertical heat flux in the equilibrium finger-driven intrusions. As discussed earlier (Section 7.1), large-scale advection by intrusions results in up-gradient heat flux: warm water is advected upward and the cold downward. Salt fingers, on the other hand, transfer heat down gradient, opposing the large-scale intrusive component. Based on tilted DNS, Simeonov and Stern (2007) conclude that (i) the net heat flux could be either upward or downward, depending on the background parameters; (ii) its large-scale and finger components are comparable in magnitude; and (iii) the presence of intrusions reduces the magnitude of the heat flux. Properties of the salt flux are markedly different. The net salt flux is dominated by the contribution from fingers and therefore is directed down gradient. Somewhat counterintuitively, the development of intrusions actually increases the net salt flux. This happens because the large-scale gradients in the salt-finger zone of a fully developed intrusion are elevated relative to the background value and so are the finger fluxes of salt. The adverse large-scale intrusion salt flux is too weak to compensate for the increased finger flux and the net salt transport with intrusions is higher than without.

The lateral heat and salt fluxes diagnosed by Simeonov and Stern (2007) are down gradient and correspond to diffusivities of $K_L \sim 2\,\mathrm{m^2\,s^{-1}}$. This value is likely to underestimate the typical interleaving diffusivities in the ocean, given that (i) for computational reasons, Simeonov and Stern employed a diffusivity ratio of $\tau = \frac{1}{6}$, significantly higher than the heat–salt value of ~ 0.01; (ii) simulations were two-dimensional, which generally under-represents the intensity of double-diffusive processes; and (iii) calculations were limited to relatively strong fronts with $a = \frac{\bar{S}_x}{\bar{S}_z} > 0.0075$ (the lateral eddy diffusivities increase with decreasing a). Nevertheless, the DNS-based predictions are invaluable for constraining the plausible range of diffusivities – the estimates reported in the literature go as high as $K_L \sim 10^3\,\mathrm{m^2\,s^{-1}}$ – and placing a lower bound on this hard-to-quantify number.

Ultimately, the lateral fluxes of heat and salt are set by the equilibrium large-scale velocity $U_{\max}$. Simeonov and Stern (2007) find that the numerical data are adequately described by the relation

$$U_{\max} = CNH, \tag{7.14}$$

where $N = \sqrt{-\frac{g}{\rho}\frac{\partial \rho}{\partial z}}$ is the buoyancy frequency, H is the intrusion thickness and $C \approx 0.14$ is the non-dimensional coefficient calibrated using a series of tilted DNS. We shall return to the discussion of (7.14) in the context of laboratory experiments and bounded models (Section 7.4).

7.4 Laterally bounded fronts

All simulations and theoretical intrusion models described so far (Sections 7.1–7.3) consider effectively unbounded fronts. The usage of the term unbounded in double-diffusive literature is somewhat loose. It is generally understood that "unbounded" implies several related conditions: (i) the front width significantly exceeds the typical intrusion wavelength, in which case, periodic lateral boundary conditions are adequate; (ii) the intrusions are controlled by the background T–S gradients; and (iii) all that happens outside the front hardly matters in terms of its effect on the intrusion characteristics. Such conditions may exist in relatively wide fronts but not in the sharp ones. Therefore, a distinct branch of intrusion theory is focused specifically on finite-width thermohaline fronts. There are a few obstacles along this path. Most notably, the simple and convenient periodic boundary conditions used for the unbounded model no longer apply. Boundary conditions are often replaced by the requirement of no flux across the frontal margins ($u = 0$ at $x = 0, L_x$) but even these should be viewed, at best, as a plausible approximation of the conditions realized in nature. On the positive side, the finite-width case can be easily modeled by laboratory experiments and is more amenable to numerical treatments.

The first rigorous, aside from minor untidiness with respect to the lateral boundary conditions, quantitative analysis of the bounded system was performed by Thorpe *et al*. (1969). Using a combination of linear stability arguments and supporting laboratory experiments, Thorpe *et al*. examined the stability of a fluid layer with vertical salinity and horizontal temperature gradients. The diffusion of properties in this configuration was due to molecular (rather than eddy-driven) fluxes, which simplified the analysis and permitted the unambiguous comparison with experiments. In contrast to the unbounded case, which is always unstable,

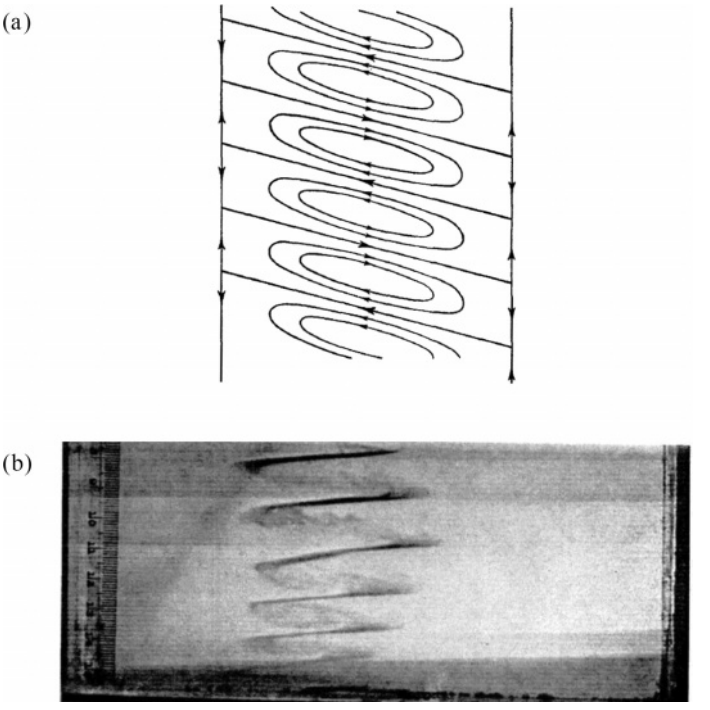

Figure 7.22 Thorpe *et al*.'s model of a thermohaline front. (a) Theoretical configuration; (b) corresponding laboratory experiments. From Thorpe *et al*. (1969).

bounded systems can be stable provided that the horizontal gradients are sufficiently weak. Thorpe *et al*. predicted marginal instability conditions and the corresponding circulation patterns, taking the form of slightly tilted intrusive structures (Fig. 7.22a).

Overall, theory and experiments agreed well. However, the experiments revealed one salient effect that was not captured by linear theory – the amalgamation of adjacent intrusions. While theory predicted the appearance of a series of cells with an alternating circulation pattern (Fig. 7.22a), the observed cells had the same sense of rotation, with the motion up (down) the heated (cold) boundary. The coalescence of adjacent cells takes place in the very early stages of development and therefore the detection and analysis of primary instabilities in experiments is difficult. Thangam *et al*. (1982) and Kerr (1990) trace the origin of the amalgamation to fundamentally nonlinear interactions that enhance the convection cells characterized by fluid rising near the heated wall and sinking at a certain distance from it. The initial effort to explain molecularly driven interleaving on fronts of finite width stimulated numerous extensions of Thorpe *et al*.'s model, of which it is important to mention the extension to a rotating system (Kerr, 1995). In the bounded configuration, the

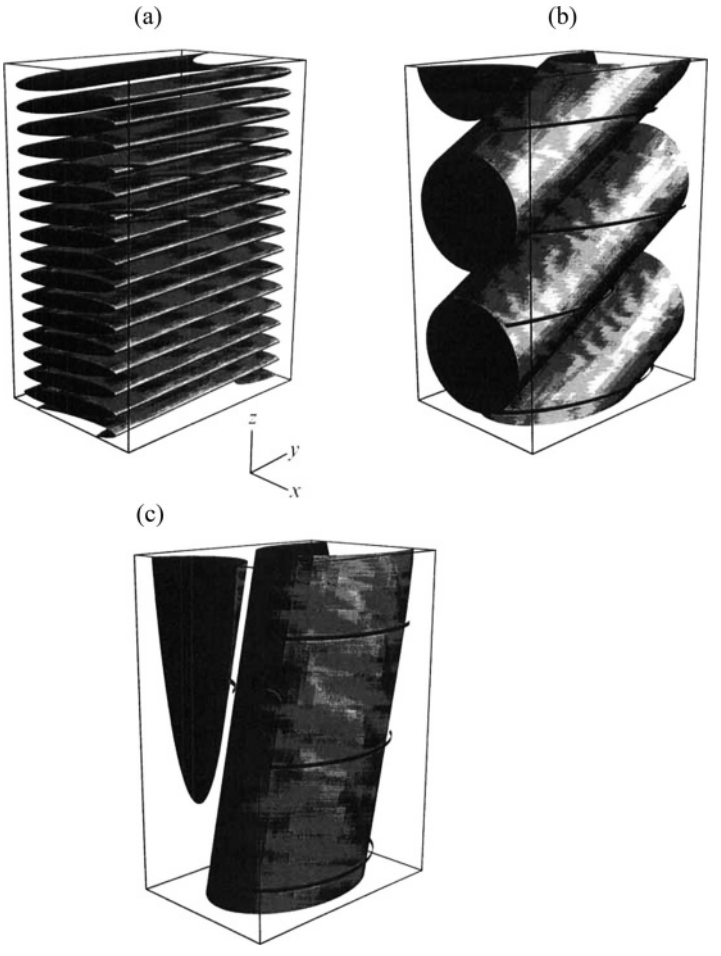

Figure 7.23 Effects of rotation on interleaving at finite-width fronts. Increase of rotation rate in (a)–(c) increases the vertical scales and slopes of intrusions. From Kerr (1995).

effects of rotation are more profound and have a generally destabilizing effect on interleaving. An increase in the rotation rates steepens intrusions in both along- and cross-front directions, as illustrated in Figure 7.23.

A counterpart to the Thorpe *et al*. (1969) analysis for salt-finger-driven intrusions was proposed by Niino (1986). Oddly enough, Niino's analysis, in contrast to Thorpe *et al*.'s model, reveals the unconditional instability of finite-width thermohaline fronts with respect to interleaving instabilities. A direct analogy between molecularly and salt-finger-driven intrusions has been generally accepted and heavily exploited in the interleaving theory, making Niino's counter-example particularly intriguing. Among numerous dynamical insights, the Niino (1986)

study reveals the significance of two key non-dimensional parameters: the stability parameter

$$R_{\text{Niino}} = \frac{\left[g(1-\gamma)\beta\Delta S_{\frac{1}{2}}\right]^6}{K_S K_M a^2 N^{10}} \tag{7.15}$$

and the stratification parameter

$$\mu_{\text{Niino}} = g(1-\gamma)\frac{\beta \bar{S}_z}{N^2}. \tag{7.16}$$

Here, $\Delta S_{\frac{1}{2}}$ is the half-difference of the salinity variation across the front, a is its half-width and $N = \sqrt{-\frac{g}{\rho}\frac{\partial \rho}{\partial z}}$ is the buoyancy frequency. The values of R_{Niino} and μ_{Niino} determine whether the front could be considered wide [for $R_{\text{Niino}} > 2 \cdot 10^5(1+\mu_{\text{Niino}})^{4.9}$] or narrow [for $R_{\text{Niino}} < 40(1+\mu_{\text{Niino}})^{5.4}$].

Niino's model assumed uniform eddy diffusivity of salt ($K_S = const$). Its long-awaited generalization, which took into account dependence of the salt-finger fluxes on the density ratio, was developed by Simeonov and Stern (2004). Using linear stability analysis and supporting numerical simulations, these authors demonstrated that finite-width thermohaline fronts can be linearly stable, provided that the lateral gradients are sufficiently weak. The critical cross-front salinity variation (ΔS_{cr}) required for instability rapidly decreases with decreasing density ratio. This result marks the second reversal of the view on the stability of weak fronts: from Thorpe *et al.* (1969) to Niino (1986) to Simeonov and Stern (2004). The disagreement between these studies is instructive. It underscores the urgent need to develop accurate physically based parameterizations of salt-finger transport.

No discussion of interleaving would be complete without reference to the Ruddick and Turner (1979) experiment. The laboratory configuration, ingenious and simple at the same time, is shown in Figure 7.24a. The lab tank was initially divided by a removable dam and both sides were filled, using the double-bucket method, with stably stratified aqueous solutes: sugar solute on one side and salt solute on the other. As in most laboratory experiments, sugar stratification (slower diffuser) represented salinity in the ocean and salt stratification (faster diffuser) – the oceanic temperature distribution. Great care was taken to ensure identical density stratification in both compartments. After the removal of the barrier, active interleaving ensued (Fig. 7.24b).

The main focus of the analysis in Ruddick and Turner (1979) was on the vertical scale of the intrusions. These authors used imaginative physical arguments based on the energetics of a thermohaline system to show that intrusion thickness is bounded from above and from below by scales proportional to $\frac{(1-\gamma)g\beta\Delta S}{N^2}$; here

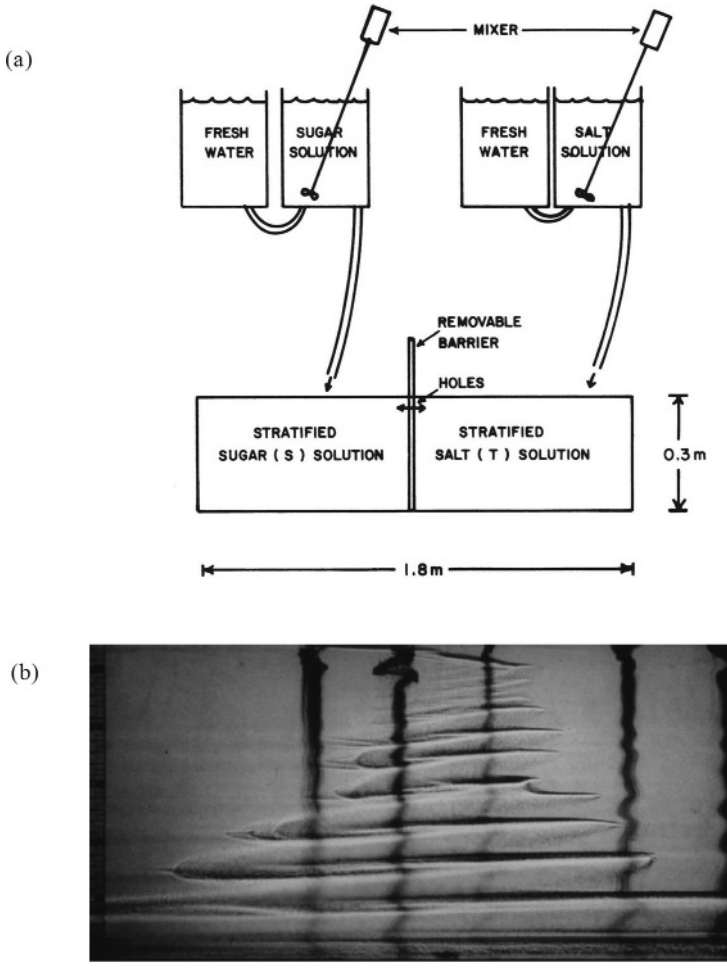

Figure 7.24 The experimental setup (a) and the resulting flow pattern (b) in Ruddick and Turner's experiments. From Ruddick *et al.* (1999).

ΔS is the lateral variation in salinity at a given level. This suggestion was validated by experiments. The best fit to the laboratory data made it possible to pin down the proportionality constant:

$$H_{\mathrm{RT}} \approx \frac{3}{2}\frac{(1-\gamma)g\beta\Delta S}{N^2}. \tag{7.17}$$

The monotonic increase in intrusion thickness towards the bottom of the tank in Figure 7.24b, where ΔS is the largest (Fig. 7.24b), is consistent with the proposed dependence of H_{RT} on ΔS. Scaling (7.17) also appears in several earlier models of finite-width interleaving (Thorpe *et al.*, 1969; Chen *et al.*, 1971). In the order-of-magnitude sense, it is equivalent to the so-called Chen scale – the height through

which a heated fluid element must rise in order to become neutrally buoyant in a given density gradient (Chen *et al*., 1971; Chen, 1974). It is also occasionally referred to as the "natural" length scale in intrusion literature (Turner, 1979).

It should be noted that the Ruddick and Turner scale (H_{RT}) is fundamentally different from the Toole and Georgi (1981) scale (H_{TG}) that emerges in the unbounded model (7.2). Such a difference is not surprising. In essence, Ruddick and Turner's experiment models intrusions in a very sharp, initially discontinuous front. In terms of frontal width (L), their experiment and the unbounded models (e.g., Toole and Georgi, 1981) represent the opposite ends of the whole spectrum of intrusion models. Niino (1986) and Simeonov and Stern (2004) demonstrated, in different ways, that the two extreme values, H_{RT} and H_{TG}, can be recovered from the finite-width model by considering the asymptotic limits of narrow ($L \to 0$) and wide ($L \to \infty$) fronts. Simeonov and Stern (2004) introduced yet another scale that is relevant for fronts of intermediate width:

$$H_{\mathrm{SS}} \sim \left(\frac{K_T L}{N}\right)^{\frac{1}{3}}, \tag{7.18}$$

and found support for it in linear and nonlinear numerical simulations.

There are many other major differences and intriguing similarities between interleaving on sharp and wide fronts. For instance, the unbounded intrusion models tend to produce step-like vertical T–S profiles with a large fraction of the intrusion occupied by well-mixed convective regions (e.g., Fig. 7.18). Such convective regions are notably absent in the Ruddick and Turner experiments (Fig. 7.24b). On the other hand, the propagation velocity of intrusions in experiments, as measured by the spreading of intrusion noses, is adequately represented by (7.14), the same relation that describes the equilibrium velocity of intrusions in the unbounded model (Simeonov and Stern, 2007). The peak velocity in the Ruddick and Turner experiments, realized at the center of the front, exceeds the nose extension velocity by a constant factor of 3.7 and therefore also conforms to (7.14). The values of the non-dimensional coefficient C are different: $C = 0.005$ for intrusion noses in the lab and $C = 0.14$ in Simeonov and Stern's simulations. However, the difference in coefficients can be readily attributed to the different molecular properties of the diffusing substances: $(Pr, \tau) = (10^3, \frac{1}{3})$ in the sugar–salt case and $(Pr, \tau) = (7, \frac{1}{6})$ in Simeonov and Stern (2007).

Intrusions in sharp fronts are inclined in the same sense as in the unbounded model, with the intrusion slope of the same sign as the slope of T and S surfaces. In a nice example of a sequel that lives up in quality to the original, Ruddick *et al*. (1999) examined mechanisms setting the geometry of intrusions in the Ruddick and Turner configuration. The essence of the Ruddick *et al*. theory lies in the hypothesis of continuous geostrophic adjustment. This hypothesis assumes that the

fluid elements in the finger region, made more (less) buoyant by the salt-finger fluxes, continuously rise (descend) to the ambient density level that matches their new density. As a result, the zero-order density distribution could be taken as horizontally uniform; the circulation in such a configuration is driven by a small perturbation to the basic adjusted state. Ruddick *et al*. (1999) demonstrate that all key experimental measurements are consistent with the theoretical model, a-posteriori validating the adjustment hypothesis. Theory in Ruddick *et al*. (1999) attributes the orientation of intrusions in sharp-front experiments to the dominance of the salt-finger transport. On the other hand, if the system is controlled by the diffusive buoyancy fluxes, the slope of intrusions is expected to be of opposite sign. Both inferences find support in oceanographic field measurements (Ruddick, 1992). With regard to the significance of the hypothesis of continuous hydrostatic adjustment, it should be mentioned that its relevance is likely to extend far beyond the intrusion problem, with numerous applications to be found in other slowly evolving buoyancy-driven systems.

The next step in the laboratory study of intrusions was made by Krishnamurti (2006). The initial state in these experiments consisted of density-compensated gradients of T and S modeled by salt and sugar solutes. The smooth horizontal gradients in Krishnamurti's setup replaced the discontinuous initial variation of T and S in Ruddick and Turner's experiment (Fig. 7.24). This change made the experimental configuration markedly more realistic – "realism" is defined in this context by dynamic similarity to typical oceanic conditions. By varying the vertical T–S gradients, Krishnamurti was able to explore interleaving in various types of background stratification: salt-finger favorable, diffusive and doubly stable. In all cases, intrusions were pronounced and visibly different from those observed by Ruddick and Turner (1979).

The most obvious difference is the presence, in Krishnamurti's experiments, of extended regions occupied by convection (Fig. 7.25). These convecting layers play a critical role in intrusion dynamics. Particle image velocimetry (PIV) has made it possible to analyze details of the velocity field, including direct calculation of the Reynolds stress. Experiments show that momentum transfer in the salt-finger zone is minimal, far less than molecular friction and thus completely negligible for most intents and purposes. Note that the same conclusion has been reached in numerical studies (e.g., Stern *et al*., 2001), leaving little doubt regarding its validity. The momentum balance is very different in the convective regions, where momentum transfer is significant and generally up-gradient, acting against molecular friction. Thus, it is the convective Reynolds stress that maintains the intrusions against viscous dissipation. A corollary of this observation is that the dynamics of intrusions in distributed fronts can be substantially different from those operating across sharp fronts (Ruddick and Turner, 1979) where convective zones are virtually absent.

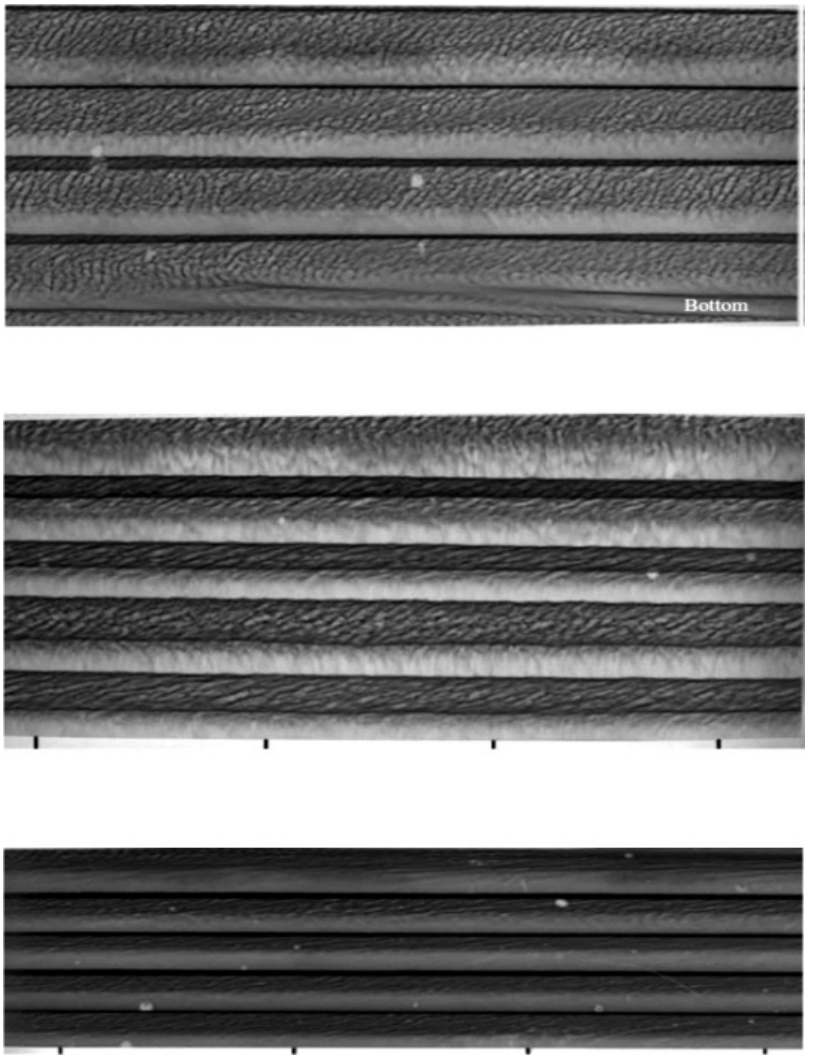

Figure 7.25 Laboratory experiments on interleaving in finite horizontal gradients. Active interleaving is observed in all configurations, including salt-finger favorable stratification (top) diffusive (center) and doubly stable (bottom). From Krishnamurti (2009).

Another distinct feature of finite-width fronts concerns the evolution of the intrusion slope. Initially, intrusions in Krishnamurti's experiments with finger-favorable stratification tilted towards the high T and S region. This is opposite to the orientation of intrusions in the Ruddick and Turner experiment, or, for that matter, in the unbounded models (Section 7.1). The "incorrect" initial inclination may be attributed to molecularly driven interleaving (Holyer, 1983). Shortly afterward, intrusions became nearly horizontal. The "correct" tilt, corresponding to the slope

of intrusions of the same sign as the slope of isotherms, was observed when intrusions entered a stable region without horizontal background gradients. Such a variation of the intrusion slope in time – not only in the magnitude but even in sign – points to a potentially serious problem for the analysis of intrusions in field measurements. If the slope of thermohaline intrusions varies dramatically even in the controlled setting of laboratory experiments, then the prospects for reliable interpretation of oceanic intrusions based on the statistics of their slope are limited. Attempts of this nature (e.g., Beal, 2007) have to be critically evaluated since the situation in the ocean is confounded by the simultaneous presence of numerous external processes: gravity waves, mesoscale variability, horizontal and vertical shears.

7.5 Sidewall heating experiments

A certain group of interleaving studies can be combined under the heading of sidewall heating (cooling) experiments. The underlying theoretical concept is one of a semi-infinite fluid forced by the temperature, and possibly salinity, flux at the boundary. In the context of laboratory or numerical experiments, this implies that the processes under consideration are sufficiently localized to the region where forcing is applied and the system is largely unaffected by the presence of distant boundaries. An argument can be made that sidewall heating experiments come closer to representing oceanic intrusions. There are no walls in the ocean interior and having only one dynamically significant boundary is, perhaps, better than having two (as in the experiments of Section 7.4). Some of the experiments by Thorpe *et al*. (1969) discussed earlier were performed in sufficiently wide containers and therefore can be placed into the sidewall heating category.

A more focused investigation was performed by Tanny and Tsinober (1988). These authors used the classical configuration (Thorpe *et al*., 1969). The working fluid, initially isothermal but vertically salt-stratified, was heated from a sidewall. However, the experimental parameters were chosen to ensure that intrusions forming near the heated boundary do not spread laterally across the whole laboratory tank but remain localized near the heated boundary throughout most of the experiment. A typical sequence of events in such experiments is illustrated in Figure 7.26. The first stage is the generation of small-scale cells with order one aspect ratio. In time, cells extend horizontally and sequentially merge, forming larger and more developed intrusions. Traces of dye in Figure 7.26 also indicate that the extent of penetration of shearing motion in the tank interior exceeds that of warm fluid that originated near the wall. The relevant scale of the intrusive layers is consistently represented by the Chen scale:

$$H_{\mathrm{C}} = \frac{g\alpha\,\Delta T}{N^2} = \frac{\alpha\,\Delta T}{\beta\,\left|\bar{S}_z\right|}, \tag{7.19}$$

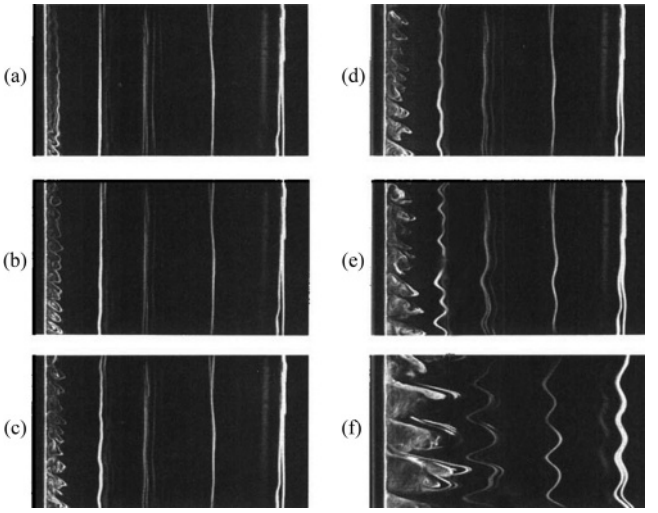

Figure 7.26 Sidewall heating experiments at various stages in (a)–(f). Note the appearance of initially small-scale slanted structures near the heated wall in (a) and (b) and their subsequent merger into the fully developed intrusions in (e) and (f). From Tanny and Tsinober (1988).

and various sidewall heating experiments suggest a relatively well-constrained range of intrusion thickness (h):

$$0.6H_{\mathrm{C}} < h < H_{\mathrm{C}}. \tag{7.20}$$

The intrusive instability in the sidewall heating experiments occurs when the Rayleigh number $R = \frac{g\alpha\Delta T H_{\mathrm{C}}^3}{\nu k_T}$ based on the Chen scale exceeds a critical value ($R_{\mathrm{cr}} \sim 1.5 \cdot 10^4$). Curiously enough, combining this observation with (7.19), we conclude that the vertical scale of the initial instabilities is

$$h_I = C\left(\frac{k_T \nu}{g\beta S_z}\right)^{\frac{1}{4}}, \tag{7.21}$$

which is analogous to the nominal double-diffusive scale d introduced in Chapter 1. The prefactor in (7.21) deduced from the laboratory experiments is $C \approx 29.1$. A more detailed analysis by Kerr (1989) suggests that the most relevant stability parameter for the sidewall heating problem is given by

$$Q = \frac{(1-\tau)^6 g(\alpha\Delta T)^6}{\nu k_S l^2 \left|\beta \bar{S}_z\right|^5}, \tag{7.22}$$

where l is the horizontal length scale, initially set by molecular diffusion of temperature from the heated boundary. Note the structural similarity of Kerr's parameter

to the stability criterion (7.15) for the salt-finger driven intrusions in bounded fronts (Niino, 1986).

If heating is strong and persistent, the sidewall temperature increases far beyond the critical value for instability and the natural scale of intrusions (7.19) increases accordingly. In this regime, the final layer thickness is expected to significantly exceed its initial value (h_I). The merging events illustrated in Figure 7.26 represent an efficient physical mechanism for the interleaving system to conform to this requirement. The mergers are initiated in the immediate vicinity of the heated wall and then spread into the interior along the intrusion fronts. A detailed inspection of mergers in the sidewall heating experiment reveals that they take one of two forms: either (i) the high-gradient interface separating intrusions weakens and eventually disappears, resulting in the coalescence of the adjacent cells, or (ii) the interface drifts vertically causing one of the intrusions to extend vertically at the expense of the adjacent one, which shrinks and ultimately disappears. Such evolutionary patterns – referred to as *B*-mergers and *H*-mergers respectively (Radko, 2007) – are common in various layered systems. Double-diffusive periodic structures just happen to be particularly susceptible to coarsening through mergers.

The "iceblock" configuration (Huppert and Turner, 1980) was designed to investigate the role of double-diffusive processes in the melting of icebergs, calved from Arctic and Antarctic glaciers. One of the goals of this study was to assess the feasibility of towing icebergs towards the coasts and harvesting the fresh meltwater from them. Who said that double-diffusers are not concerned by societal needs? In Huppert and Turner's experiment, the iceblock was vertically inserted into salt-stratified water at rest. Despite different geometry and boundary conditions (in addition to thermal forcing, melting ice also produces the associated freshwater flux) dynamic similarities between the iceblock and sidewall heating experiments are apparent. Shortly after insertion of the iceblock, the flow pattern became dominated by the laterally spreading intrusions (Fig. 7.27, top panel). The intrusions tilt slightly upward, away from the iceblock, which is consistent with the dominance of fluxes across sharp diffusive interfaces in the strongly diffusive background stratification. Interleaving persisted even after the removal of the iceblock (Fig. 7.27, bottom panel) although the intrusions became more horizontal and voluminous. What is particularly striking is the extent to which quantitative inferences from the sidewall heating studies apply to the iceblock experiment. For instance, the thickness of intrusions measured by Huppert and Turner falls within the sidewall heating range (7.20). The laboratory-based predictions find support in field measurements taken in the vicinity of Antarctic glaciers (Jacobs *et al.*, 1981). Such agreement is yet another indication of the very robust physics of interleaving.

During the past three decades, numerous other extensions of the sidewall heating problem have been considered. Quite a few questions have been answered, many

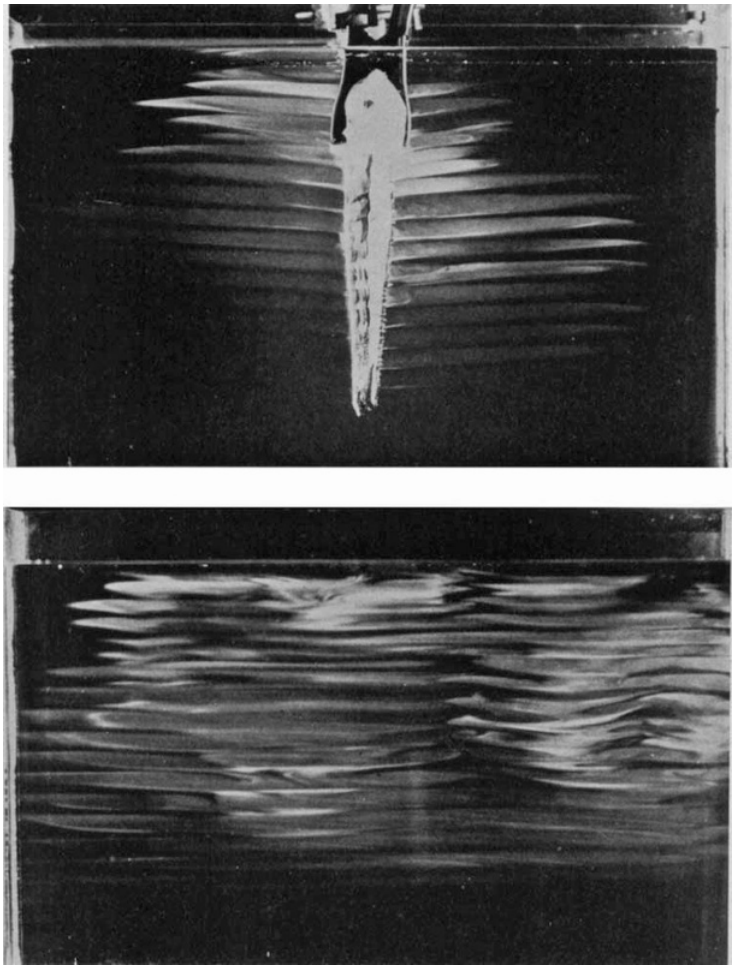

Figure 7.27 Melting iceblock experiment. Dye has been frozen into the ice to visualize ensuing interleaving motions. The top panel shows the state after inserting the iceblock and the bottom panel after its removal from the tank. From Huppert and Turner (1980).

more remain. Our intention is not to review here all aspects of sidewall heating but rather to convey a sense of the interesting and rich dynamics of the problem. Still, some key developments should be highlighted:

(i) A series of papers examined intrusions developing from localized sources, such as heating at a point (Tsinober *et al*., 1983; Belyaev and Chashechkin, 1989; among others) or injection of fluid with anomalous properties (e.g., Turner, 1978; Nagasaka *et al*., 1995);

(ii) Narusawa and Suzukawa (1981) and Schladow *et al*. (1992) imposed a fixed heat flux, instead of the temperature difference in classical experiments, and examined ramifications of this change for stability of the system;
(iii) Huppert *et al*. (1984) performed a series of sidewall heating experiments with various substances and discovered that intrusions are largely insensitive to molecular characteristics (Pr and τ);
(iv) Chereskin and Linden (1986) explored the (limited) effects of rotation on sidewall heated intrusions;
(v) Chen and Chen (1997) studied salt fingers developing in the convection cells and emphasized the importance of incorporating finger-driven fluxes into theoretical models of sidewall heated intrusions;
(vi) Dijkstra and Kranenborg (1998) and Kranenborg and Dijkstra (1998) reproduced key features of laboratory experiments using two-dimensional numerical simulations;
(vii) Chan *et al*. (2002) used laboratory experiments to examine the three-dimensional structure of intrusions associated with the appearance of secondary horizontal recirculation cells;
(viii) Malki-Epshtein *et al*. (2004) examined the effects of a distant wall on the propagation of intrusions and quantified conditions for which the tank length appears as an important variable.

Perhaps the most important message that we can take from this extensive body of literature is that interleaving in sidewall heating experiments is not particularly sensitive to the specifics of each setup. The general evolutionary patterns of intrusions, their geometry and mechanics, exhibit strong similarities across various experimental configurations and parameter regimes. Of course, quantitative differences exist. They are interesting and should be investigated further. However, it is comforting to know that major insights into intrusion dynamics are likely to be transferable between different systems. In the next section we shall discuss to what extent these insights might be relevant for interleaving in the ocean.

7.6 Oceanographic observations

Given all the effort invested in theoretical, laboratory and numerical modeling of interleaving, given the elegant and generally consistent physical picture that emerges, it is incredibly tempting to apply our hard-won understanding directly to all intrusive structures in the ocean. But is it reasonable to assume that the dynamics of oceanic intrusions are, in most cases, governed by the same physical principles as intrusions in the laboratory and theoretical models? Remarkably, after almost

a half-century of theorizing, modeling and observing, we are still in doubt. The lack of definitive answers cannot be attributed to the rarity of the phenomenon. On the contrary, intrusions are ubiquitous; almost any temperature and salinity profile in the world ocean contains inversions indicative of lateral thermohaline intrusions. It is also not because of insufficient effort. A decade-old review of observations (Ruddick and Richards, 2003) already referred to 156 predominantly field-based studies of interleaving. The principal difficulty is that there are a number of processes – mesoscale variability, external shears, internal waves, to name a few – that can potentially produce intrusions in the ocean or at least substantially affect their evolution. These factors are a-priori excluded in the majority of idealized studies. We know that double-diffusion is responsible for interleaving in Ruddick and Turner's experiments; there is nothing else to blame. Nature is more diverse and complicated.

Of course, there are several well-known examples of interleaving for which observational evidence of their double-diffusive origin is undeniable and the dynamics are adequately captured by conventional theories. We shall present such cases first. These success stories will be followed by more controversial observations, which seem to contradict, at least in some respects, the basic double-diffusive theory of interleaving; alternative explanations will be discussed. The section ends with the list of considerations that we believe should be taken into account to reconcile oceanographic measurements with theoretical models.

Success stories

While interleaving is widespread in the world ocean, much observational effort for its detection is focused on regions characterized by strong lateral gradients of temperature and salinity. There are several reasons for that. Since interleaving is driven by lateral gradients of temperature and salinity, it is natural to expect it to be more active in areas where the gradients are large. At the same time, property contrasts between adjacent intrusions are higher if interleaving occurs at a boundary between distinct water masses, which helps to identify and analyze interleaving in field measurements. Finally, the critical large-scale consequences of interleaving may be related to its ability to diffuse sharp lateral gradients (Garrett, 1982; Schmitt, 1994b). It is generally accepted that the ocean is actively stirred by mesoscale (10–100 km) eddies driven by baroclinic instability. Mesoscale variability, however, does not result directly in irreversible mixing but, rather, acts as a catalyst by transporting tracers towards high-gradient fronts where mixing is finalized by some irreversible diabatic processes. Interleaving may represent this elusive "missing link" between adiabatic mesoscale stirring and the ultimate destruction of T–S variability by molecular dissipation.

The largest lateral gradients in the ocean are generally found in (i) quasi-permanent frontal regions separating global-scale water masses and (ii) isolated coherent vortices, which are able to transport a substantial volume of trapped fluid into regions with distinct ambient temperature and salinity properties. A clear example of frontal interleaving, supplemented by its comprehensive analysis, is given by Joyce *et al.*'s (1978) observations of the polar front of the Antarctic Circumpolar Current in the Drake Passage. Within the front, water masses were observed to intrude with characteristic vertical scales of 50–100 m. Joyce *et al.* argue that at least three features of the observed intrusions are consistent with double-diffusive dynamics: the vertical buoyancy flux is up-gradient; the intrusions tilt in the direction expected for salt-finger driven interleaving; and the pattern of vertical stratification conforms to the structure of typical thermohaline intrusions. A number of studies (Joyce, 1976; Williams, 1981; Schmitt and Georgi, 1982) document intrusive fine-structure across the Gulf Stream and North Atlantic Current and provide evidence for their salt-finger driven dynamics.

Some of the most spectacular examples of interleaving come from the Arctic regions where, due to the relatively low energy environment, double-diffusion could be a dominant mechanism for vertical and, through interleaving, horizontal mixing. An abundance of well-defined intrusions, extending laterally for hundreds of kilometers, is a characteristic feature of the Arctic environment. In the Arctic, intrusions have been observed in all types of background stratification: salt-finger favorable, diffusive and double-diffusively stable. While density stratification is stable, vertical temperature and salinity profiles are frequently characterized by zigzag patterns with numerous inversions – the tell-tale sign of thermohaline interleaving. Representative examples are shown in Figure 7.28 (measurements in the Laptev Sea, Rudels *et al.*, 2009). The instantly recognizable signatures of interleaving also appear in the *T*–*S* diagram (Fig. 7.28, bottom right): properties vary in a coherent manner consistent with their partial density-compensation. The very sharp features of all profiles in Figure 7.28 are also indicative of active double-diffusive processes; small-scale turbulence is generally characterized by the opposite smoothing tendency. Estimates of lateral diffusivities associated with intrusions are in the range of 100–1000 m s^{-2}, significantly exceeding that for mid-latitude interleaving. The ability of intrusions to profoundly affect high-latitude circulation has been emphasized by several studies (Perkin and Lewis, 1984; Walsh and Carmack, 2002; Rudels *et al.*, 2009). Of particular importance for the Arctic climate is the role of interleaving in mixing water masses of Pacific (colder and fresher) and Atlantic (warmer and saltier) origin (Carmack *et al.*, 1997; Rudels *et al.*, 1999).

A number of field studies report active interleaving in isolated coherent vortices. The most convincing example of this type is presented by meddy Sharon, one of

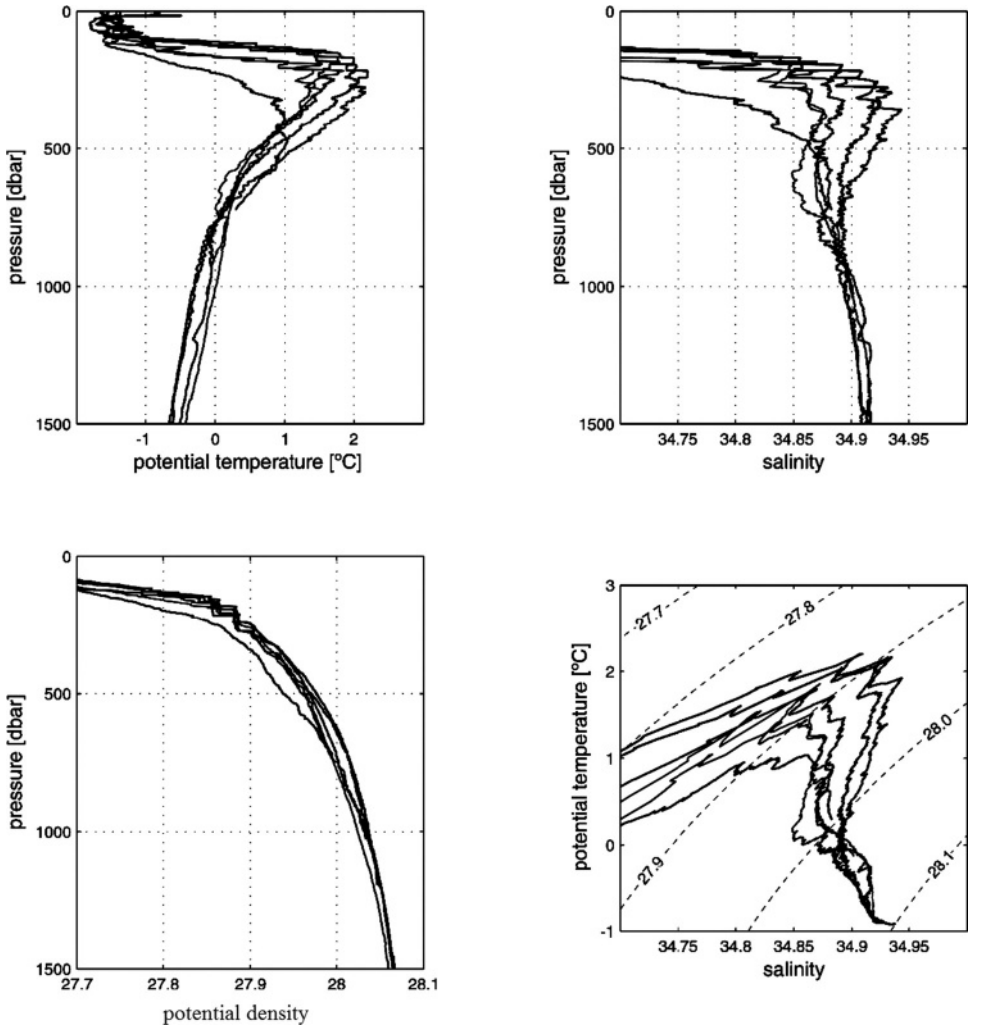

Figure 7.28 Arctic intrusions. Typical vertical profiles of potential temperature (top left), salinity (top right), potential density (bottom left) and the temperature-salinity diagram (bottom right) all exhibit numerous density-compensated inversions. From Rudels *et al.* (2009).

the intra-thermocline lenses of Mediterranean origin, which was systematically observed in the North Atlantic from 1984 to 1986. Sharon died a horrible death – she was eaten alive by thermohaline intrusions. The gradual erosion of heat, salt and velocity signatures was well documented and has been the subject of extensive analyses (Armi *et al.*, 1988, 1989; Hebert *et al.*, 1990; Ruddick, 1992, Ruddick *et al.*, 2010; May and Kelley, 2002). Stratification in the upper (lower) part of the meddy was diffusively (salt-finger) favorable, as shown in Figure 7.29a. Vertical diffusion

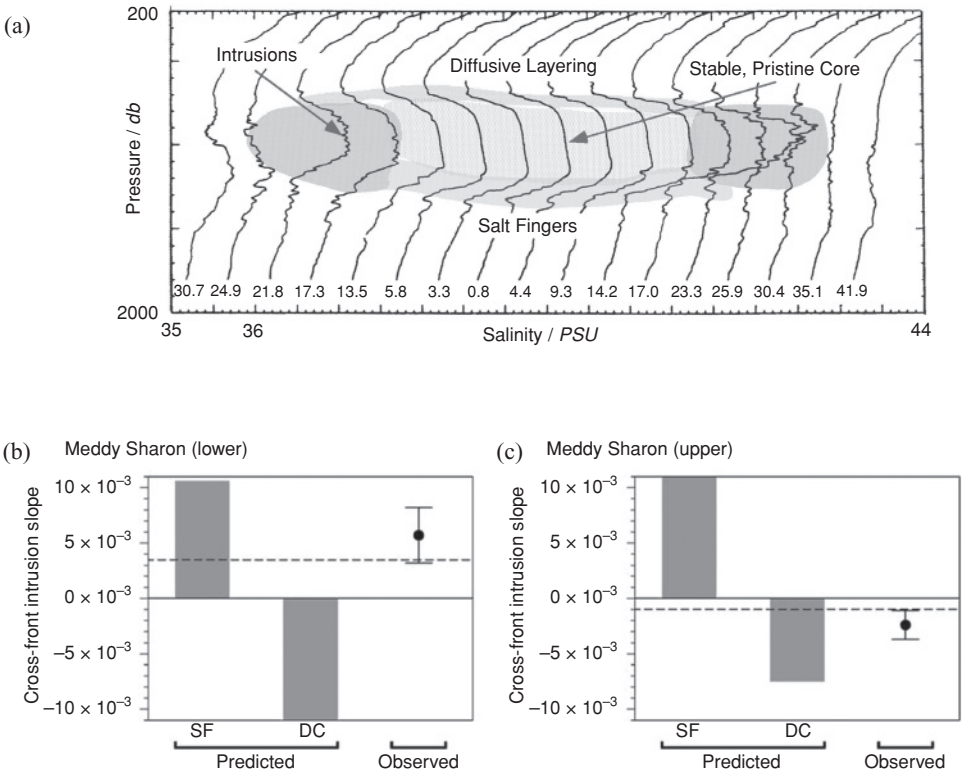

Figure 7.29 Observations of meddy Sharon. (a) Salinity structure (from Ruddick *et al*., 2010). The range of intrusion slopes predicted on the basis of interleaving theories along with the observed values for the lower (b) and upper (c) parts of the meddy (from May and Kelley, 2002).

by itself was clearly insufficient to account for the observed erosion rates. The exclusion of lateral exchanges in the meddy heat/salt budget would lead to decay time scales of about twenty years, an order of magnitude underestimate (Hebert, 1988). This mismatch led to the suggestion that thermohaline intrusions, active and abundant at the meddy front (Fig. 7.29a), could be the primary mixing agent. The overall structure of intrusions and their slopes (Fig. 7.29b) were consistent with their double-diffusive origin in both diffusive and salt-finger regions. Predominantly baroclinic mechanisms (McIntyre, 1970) have been unambiguously ruled out (Ruddick, 1992). The vertical scales of intrusions and their advective velocities were in agreement with the predictions based on the sharp front model (Ruddick and Turner, 1979; Ruddick *et al*., 1999).

An even more definitive calculation was made by Ruddick *et al*. (2010). Building on an earlier proposal (Joyce, 1977), Ruddick *et al*. utilized measurements of thermal microstructure to quantify interleaving-driven lateral mixing. The model

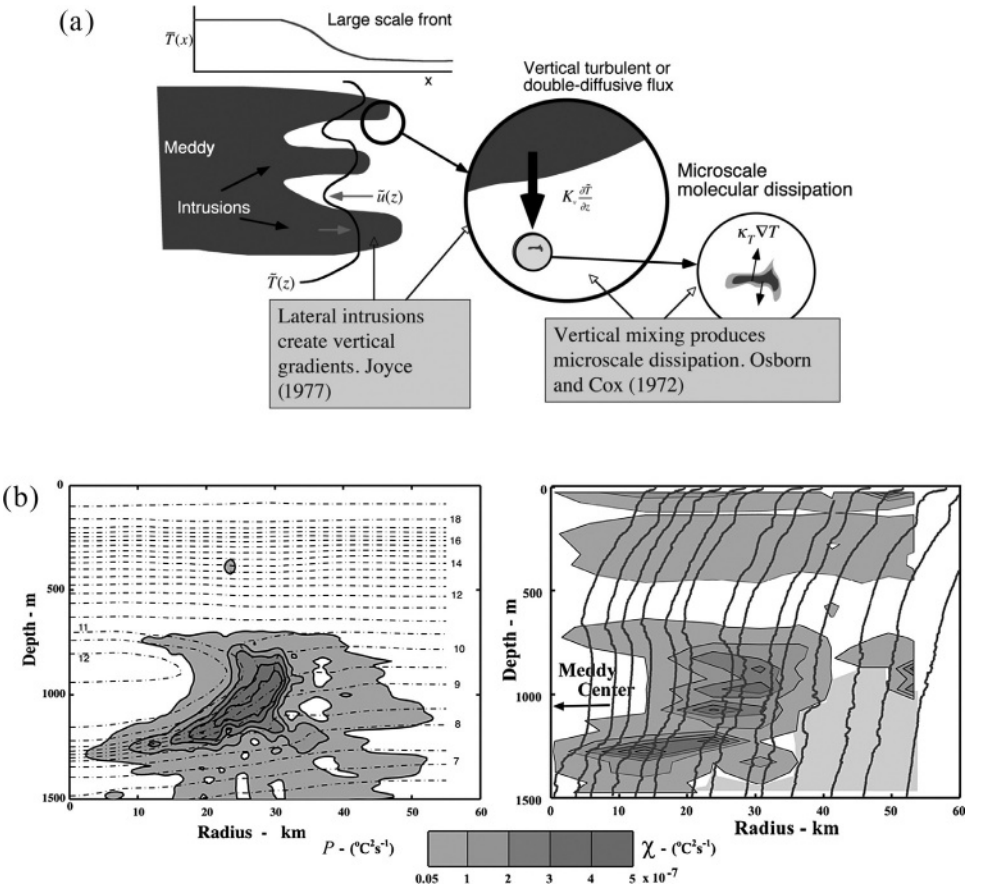

Figure 7.30 (a) Schematic illustration of the link between the production of thermal variance by the lateral interleaving motions and its ultimate dissipation by the microstructure. (b) Comparison of the production terms based on the erosion rate of meddy Sharon (left) with the microstructure dissipation (right). From Ruddick *et al*. (2010).

was based on the temperature variance equation, which under assumptions of statistically steady state and homogeneous turbulence reduces to the balance between advective variance production and molecular dissipation:

$$P = -2\overline{\vec{v}'T'} \cdot \nabla \bar{T} = 2k_T \overline{|\nabla T'|^2}, \tag{7.23}$$

where $\bar{T}$ represents the large-scale temperature distribution on scales greatly exceeding the dimensions of individual intrusions – see the schematic in Figure 7.30a. Joyce (1977) assumed that in regions of active interleaving the production term is dominated by the horizontal component associated with

interleaving. Temperature variance is ultimately dissipated on the microscale (∼cm), which reduces (7.23) to

$$P \approx -2\overline{u_i T_i}\frac{\partial \bar{T}}{\partial x} \approx 6k_T\overline{\left(\frac{\partial T_m}{\partial z}\right)^2}, \tag{7.24}$$

where subscripts i and m pertain to the intrusion and microstructure scales respectively. Note that (7.24) also assumes isotropy of microstructure, $\overline{\left(\frac{\partial T_m}{\partial x}\right)^2} \sim \overline{\left(\frac{\partial T_m}{\partial y}\right)^2} \sim \overline{\left(\frac{\partial T_m}{\partial z}\right)^2}$, a questionable but rather conventional step in observational mixing studies (Osborn and Cox, 1972).

Equation (7.24) makes it possible to evaluate the lateral production term $P = -2\overline{u_i T_i}\frac{\partial \bar{T}}{\partial x}$ from high-resolution microstructure measurements taken during the 1985 survey of meddy Sharon. The outward heat transport was estimated directly from the erosion rates of the meddy. These two completely independent estimates agreed nicely: not only typical values of P but their spatial distribution matched (Fig. 7.30b). This agreement is significant. First of all, it leaves no doubt that the erosion of the meddy should be attributed to thermohaline interleaving. It also validates key assumptions of Joyce's (1977) interleaving model: (i) the production of thermal variance in strong fronts is dominated by its horizontal component and (ii) the production–dissipation balance is satisfied even in the local sense.

Several attempts have been made to analyze interleaving in other coherent vortices. The results are encouraging but not as clear-cut as for Sharon. Schmitt *et al.* (1986) reported observations of intrusions at the edge of a warm-core Gulf Stream ring. Their fine- and micro-structure measurements revealed clear signatures of double-diffusive mixing. Intrusions were found to slope in the diffusive sense, which is consistent with microstructure data showing that diffusive interfaces in this ring were more unstable and had higher turbulence levels than nearby fingering regions. More quantitative comparisons were precluded by the complex three-dimensional structure of the intrusive features associated with wrapping of "streamers" of shelf, slope and Gulf Stream waters around the ring. The situation was further complicated by vertically sheared advection and high levels of mechanically generated turbulence.

Observations of thermohaline structures in the ocean have been invigorated in recent years by a new and highly promising technology – multichannel seismic imaging. Seismic imaging, which has been used by geophysicists for decades in the analysis of the Earth's subsurface, can also be used to display oceanic fine-structure in unprecedented detail (Holbrook *et al.*, 2003). In a seismic survey, sound is sent from a ship-towed source, reflected by water masses with significant

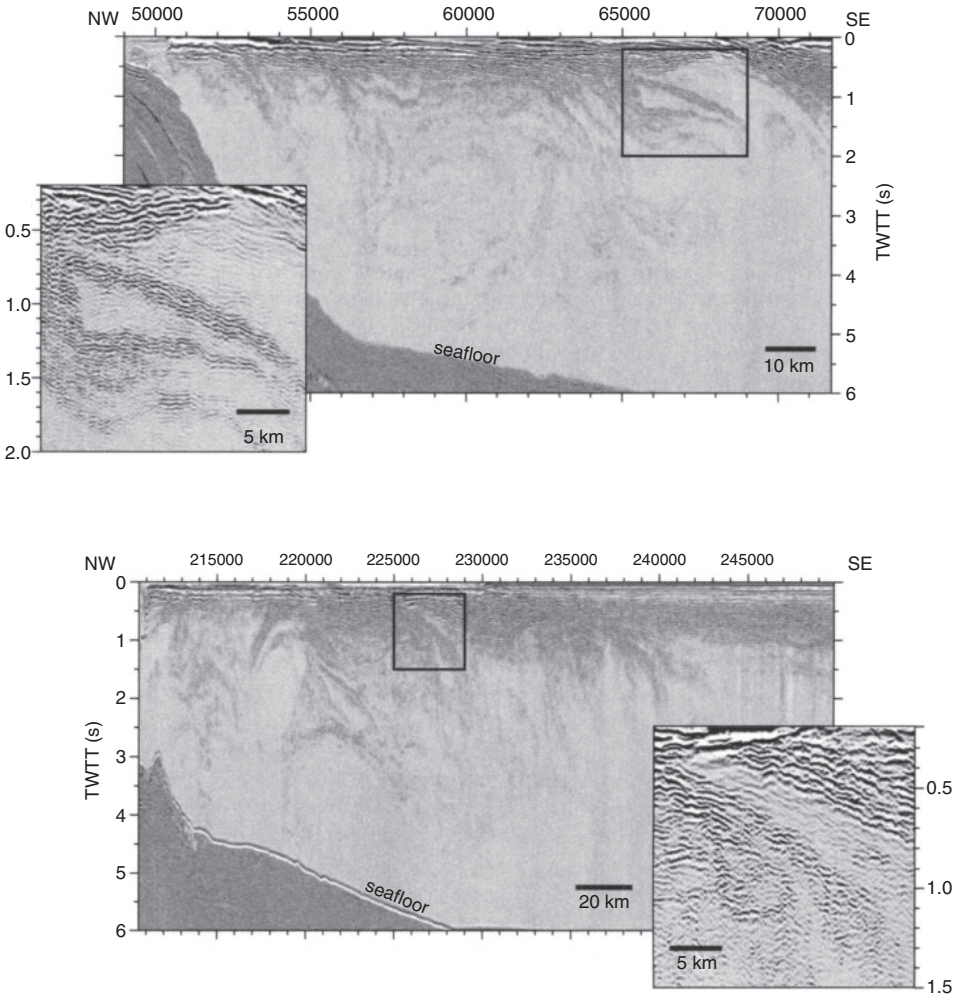

Figure 7.31 Seismic images off the coast of Newfoundland. Insets show an enlarged image of coherent slabs penetrating to ~1000 m depth, indicated by the corresponding boxed areas. From Holbrook *et al*. (2003).

temperature and salinity anomalies, and received by an array of towed hydrophones. The acoustic signal is then processed to map the thermohaline structure to depths of 1 km or more. The resolution attained by seismic imaging is on the order of 10 m in the vertical and approximately 100 m horizontally, which makes this technique perfectly suited for representation of secondary double-diffusive structures – intrusions and staircases. The acoustic impedance is affected by temperature and, to a lesser extent, by salinity. Therefore, seismic images could be interpreted as scaled maps of the temperature gradient (Ruddick *et al*., 2009). Figure 7.31

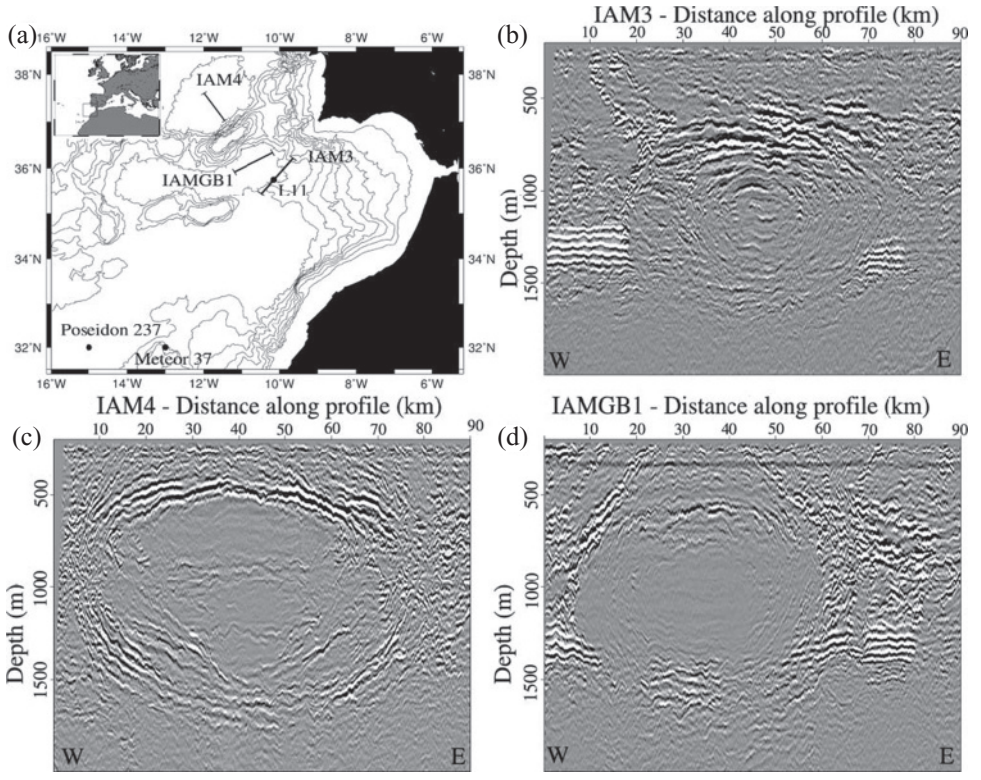

Figure 7.32 Thermohaline interleaving in meddies. (a) Map showing the geographical location of the study zone. Lines indicate the position of the multichannel seismic (MCS) profiles taken during the Iberian–Atlantic Margin (IAM) survey. MCS images of profiles (b) IAM3 on August 31, (c) IAM4 on August 29 and (d) IAMGB1 on September 7. From Biescas *et al*. (2008).

presents some of the first seismic images (Holbrook *et al*., 2003). Clearly visible in these images is a series of well-defined laterally coherent intrusions that occupy a significant fraction of the upper ocean. The observational location at the front separating Gulf Stream from colder and fresher Labrador waters, as well as the characteristic finescale patterns, is consistent with the double-diffusive origin of interleaving (Ruddick, 2003).

Another promising location for the seismic analysis of intrusions is at the peripheries of meddies. Strong temperature and salinity variations between their interior and surrounding waters create perfect conditions for double-diffusive interleaving, as was illustrated earlier in the example of meddy Sharon. At the same time, temperature contrasts are associated with high reflectivity, which makes seismic images of meddies (Biescas *et al*., 2008) most spectacular. The relatively homogeneous central parts of meddies (Fig. 7.32) are only weakly reflective. These core regions

are surrounded by strong reflectivity bands suggestive of active interleaving. Intrusions are numerous and well-defined; they spread laterally, exchanging properties between the meddy interior and surrounding waters. The proposition of the ultimate demise of meddies through interleaving mechanisms becomes all the more convincing in view of these new seismic observations. The images in Figure 7.32 also reveal systematic differences between layers developed at the upper and lower meddy boundaries, apparently reflecting their different types (diffusively driven above and finger-driven below the core).

Song *et al*. (2011) performed an even more detailed analysis of seismic images of water masses in and around a newly discovered meddy in the Iberian Basin off the coast of Portugal. This study led to intriguing insights into the interplay between thermohaline interleaving and eddy stirring in the cascade of thermal variance to microscale dissipation. Seismic observations revealed that thermohaline intrusions are concentrated in isolated bands, associated with anomalously high mixing. These bands were interpreted as "spiral arms" of water, removed from the meddy periphery by mesoscale stirring. The structure of finescale intrusions in the spiral arms was fully consistent with their double-diffusive origin and inconsistent with direct mesoscale stirring. It was argued that the partnership between eddy stirring and thermohaline intrusions is an essential element in a chain of mixing processes in the Iberian Basin. Stirring produces strong lateral fronts; these fronts become sites of spontaneous interleaving and are ultimately dissipated by intrusion-driven mixing.

Admittedly, most current applications of seismic oceanography are inherently descriptive. However, there is significant interest in developing this technology into a source of quantitative information (e.g., Paramo and Holbrook, 2005; Sheen *et al*., 2009) that can match conventional data in terms of accuracy and unambiguous interpretation. Regardless of the outcome of such efforts, the significance of the insights that seismic imaging provides into the finescale stage of mixing is already evident. These images convey a powerful sense of the omnipresence and intensity of interleaving – that ominous tangle of squirming serpents jumbled together in the snake-pit of the ocean. This sense is blunted in more conventional oceanographic observations.

Alternative arguments

As we have seen in the foregoing examples, double-diffusion can produce strong intrusive motions provided that it is the dominant mixing agent at a given location. In such cases, interleaving is active; it profoundly affects water-mass distribution and circulation patterns on much larger scales. However, it is not clear what happens if double-diffusion is absent, weak or dominated by some other mixing

process present at the same location. Can we still expect interleaving of substantial magnitude and characteristic intrusive-like structure? The answer to this question is "maybe."

The most intriguing in this regard are observations of intrusions in double-diffusively stable regions – the regions where vertical background *T*–*S* gradients support neither salt fingering nor diffusive convection. The initiation of intrusions in such conditions requires mechanisms that are not represented in conventional intrusion theories (Stern, 1967; Toole and Georgi, 1981). And if the origin of intrusions is non-thermohaline, it becomes questionable whether double-diffusion is essential for their maintenance. One possibility is that the first stage of interleaving is the development of molecularly driven intrusions (Chapter 2), which can grow in lateral gradients regardless of vertical stratification (Holyer, 1983; Stern, 2003; Thompson and Veronis, 2005). When the amplitude of intrusions is large enough to create inversions in vertical *T*–*S* profiles, double-diffusive mixing takes over. The vertical scale of the fastest growing molecularly driven intrusions is much less than the scale of intrusions typically observed in the ocean. However, shortly after formation, molecularly driven intrusions start to merge sequentially, which can increase their thickness to the observed levels (Simeonov and Stern, 2008).

An alternative scenario was proposed by Hebert (1999), who attributed interleaving in stable regions to the action of differential diffusion. In the case of incomplete turbulent mixing (supposedly caused by overturning gravity waves), eddy diffusivity of heat can exceed that of salt. Since molecular *T*–*S* diffusivities are different ($k_T \gg k_S$), some turbulent events of limited duration would effectively mix temperature but not salinity. If effective diffusivities of heat and salt are different, spontaneous interleaving is once again possible, which can be shown by straightforward reinterpretation of the classical theory (Stern, 1967). Merryfield (2002) applied the intrusion model to observations of the Upper Polar Deep Water in the Arctic (Anderson *et al*., 1994) and found that the differential diffusion model is not inconsistent with observations. Kuzmina *et al*. (2011) reexamined the differential diffusion mechanism of interleaving using data from the Eurasian Basin and suggested that it remains a viable explanation for the observed intrusions in doubly stable regions. This study emphasized the significance of baroclinic effects in controlling the intrusion slopes and intensity of interleaving in the differential mixing model. The lateral diffusivities in doubly stable regions were estimated to be in the range of 17–57 $m^2\ s^{-1}$. Intrusion-driven mixing of such strength constitutes an important mechanism for water-mass transformation, particularly in view of weak internal wave activity in the Arctic Ocean.

Both scenarios, molecular interleaving and differential diffusion, could still be broadly described as double-diffusive. The difference in molecular diffusivities

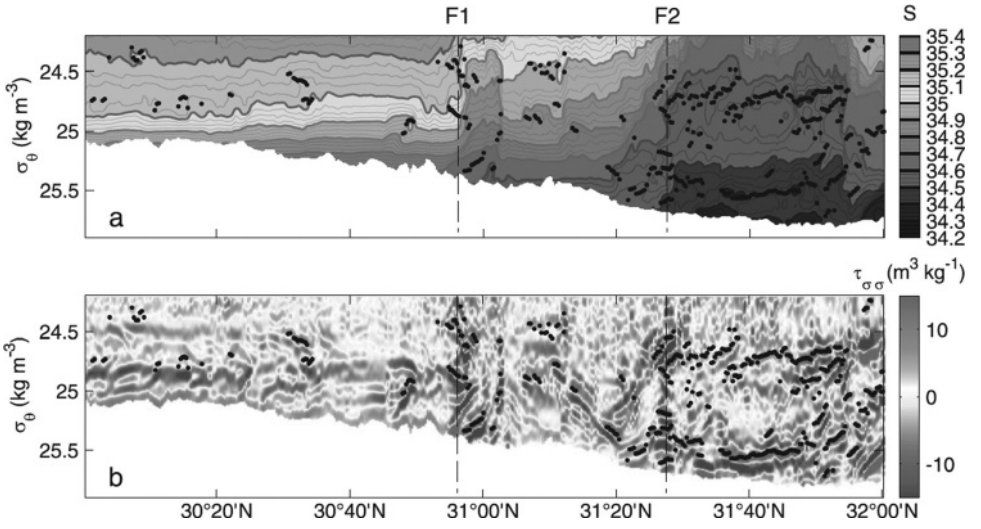

Figure 7.33 The vertical sections of salinity (a) and curvature of spiciness (b) at the North Pacific Subtropical Frontal Zone. The spiciness diagnostics reveal the presence of numerous intrusions that have very limited expression in terms of salinity. From Shcherbina *et al*. (2009). See color plates section.

of heat and salt is essential. However, completely different possibilities have been considered. For instance, Shcherbina *et al*. (2009) examined thermohaline intrusions in the North Pacific Subtropical Frontal Zone (NPSFZ). This region is only mildly susceptible to salt fingering ($R_\rho > 2$). Interleaving is also less active or, at least, less visible. Generally, fully developed interleaving is easily detectable by inversions of temperature and salinity (e.g., Fig. 7.28). Detection of intrusions at the NPSFZ required more sophisticated diagnostics, based on a water-mass characteristic called spiciness. Spiciness (τ) can be defined through its differential as

$$d\tau = \rho(\alpha dT + \beta dS). \tag{7.25}$$

In terms of thermal and haline components (αT and βS), spiciness is orthogonal to density, which makes it a rather sensitive indicator of variations in water-mass composition. The second derivative of spiciness with respect to potential density ($\tau_{\sigma\sigma}$) accentuates such variations even more. Numerous intrusive structures that are too weak to have a visible impression on the salinity distribution (Fig. 7.33a) are clearly revealed by the pattern of $\tau_{\sigma\sigma}$ (Fig. 7.33b).

The analysis of intrusion patterns by Shcherbina *et al*. was inconclusive – the range of the observed intrusion slopes was much broader than could be expected on the basis of classical theories; slopes of both signs were observed. Shcherbina *et al*. (2009) hypothesized that intrusions at this location are not self-driven but

produced by "passive" mechanisms, associated with stirring of thermohaline gradients by mesoscale eddies. This argument hinges on two fundamental properties of rotating stratified turbulence – inverse transfer of energy and density towards large vertical scales and direct transfer of *T*–*S* variability to relatively small scales. As a result, mesoscale eddies are expected to be ineffective in creating density variability on intrusion scales (∼10 m). Temperature and salinity, on the other hand, could vary significantly, albeit in the coherent density-compensated manner (Ferrari and Polzin, 2005; Smith and Ferrari, 2009). While the idea is certainly interesting, it is clear that much more detailed analyses, theoretical and observational, are required to quantify the role of passive processes in the dynamics of interleaving under various thermohaline conditions. Song *et al*. (2011) argued against the "passive interleaving" mechanism by noting that the slopes of most intrusive features observed in seismic images of oceanic fine-structure are much flatter than expected for interleaving driven directly by mesoscale stirring.

Another version of the passive interleaving hypothesis invokes internal waves as the ultimate driver of intrusive motions. In its simplest form, the idea was originally suggested by Georgi (1978). Georgi envisioned slow inertial waves with nearly horizontal velocity that varies vertically in a periodic manner. The resulting vertically sheared motion would differentially advect properties across lateral thermohaline fronts creating a *T*–*S* imprint that is oscillatory in the vertical and is horizontally extended – something that does resemble intrusions. This hypothesis in its raw form is easy to refute. First of all, internal waves periodically reverse displacements. The lifetime of intrusions is uncertain but it definitely exceeds the period of near-inertial waves (∼1 day). In addition, Joyce *et al*. (1978) ruled out internal waves as a source of interleaving by comparing the amplitudes of temperature and velocity in the observed intrusions. This ratio was very different, by at least two orders of magnitude, from what could be expected for wave-driven perturbations. Still, Georgi's suggestion cannot be dismissed entirely. Even if waves do not cause interleaving directly, it does not necessarily mean they are not important.

The thirty-year pause in the debate on this topic was recently interrupted by the laboratory study of Griffiths and Bidokhti (2008). In their experiments, two buoyant plumes were released into the opposite ends of a long channel filled with water. The immediate consequence of such forcing was the generation of internal waves, which was followed by the appearance of lateral intrusions, clearly visible in Figure 7.34. The experiments were performed in both single-component (Fig. 7.34a) and two-component (Fig 7.34b) stratifications. Remarkably, the outcomes of these experiments were very similar; salt fingers appearing in the double-diffusive case (Fig. 7.34b) had almost no effect on the magnitude and

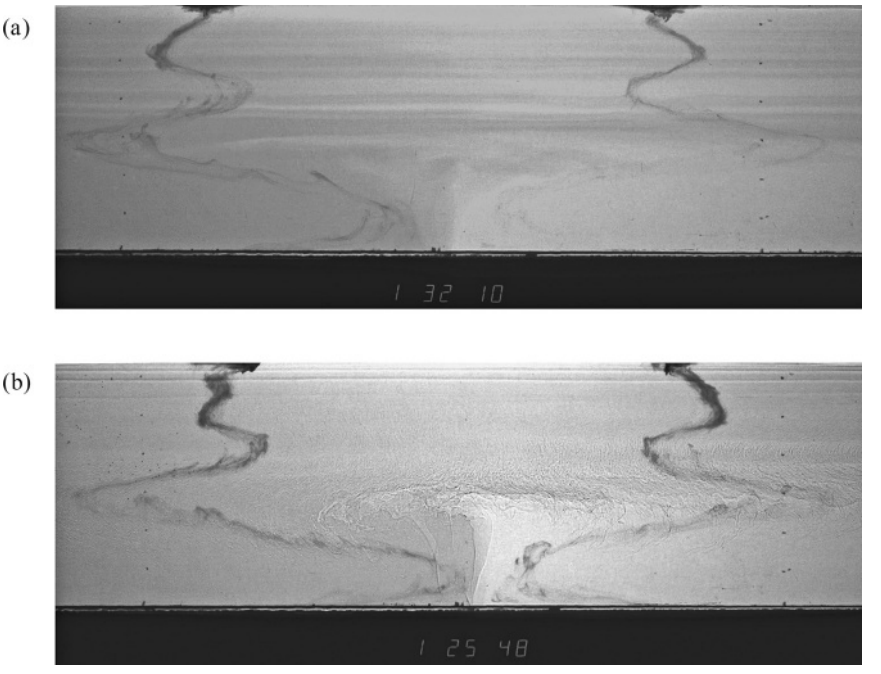

Figure 7.34 Intrusions generated by releasing buoyant plumes into a long channel filled with one-component (top panel) and double-diffusive (bottom panel) fluids. From Griffiths and Bidokhti (2008).

pattern of intrusions. The authors attributed interleaving to the action of internal waves. This mechanism undoubtedly involves nonlinear interactions between various modes of internal waves. However, the precise mechanics of such interaction, as well as its relevance to interleaving in the ocean, remain unclear.

Our final example of an ambiguous and poorly understood set of observations (those are kind of fun, aren't they?) concerns equatorial interleaving. A number of studies (Toole, 1981; Richards and Banks, 2002; Lee and Richards, 2004) have reported observations of intrusions in the equatorial Pacific thermocline. The interleaving signatures there are unmistakable. Characterized by vertical scales of a few tens of meters and laterally coherent over hundreds of kilometers, these intrusions are as formidable as one can find in the world ocean. The lateral heat transfer by equatorial interleaving can substantially affect the temperature distribution in the tropical thermocline and the speed of the equatorial undercurrent (Pezzi and Richards, 2003). Given their potential large-scale impact, it is imperative to identify the mechanisms for establishment and maintenance of equatorial intrusions. In addition to the general oceanographic interest, identification of their origin is essential for the development of physically based parameterizations of interleaving

in large-scale numerical and theoretical models. The biggest problem here is that, in addition to thermohaline mechanisms, equatorial intrusions could also be generated by inertial instabilities. Edwards and Richards (1999, 2004) argue that both processes produce similar T–S signatures, which makes it difficult to discriminate between them on the basis of observations. But wait, things get even more complicated. In certain parameter regimes, inertial and thermohaline modes interact, resulting in the mixed thermohaline–inertial instability (Edwards and Richards, 1999). The presence of such mixed modes may preclude identification of a single dominant player in equatorial interleaving. In addition to the Pacific, vertically periodic layered structures have also been observed in the equatorial Atlantic, where they also could be associated with inertial instabilities, thermohaline processes or some combination thereof (D'Orgeville *et al*., 2004). The problem of equatorial interleaving is complicated and remains largely unresolved.

Complications

There is no doubt that our understanding of interleaving and the general interest in this field have grown substantially in recent years. Continuous developments of the classical theory – inclusion of baroclinicity, effects of background turbulence, and more physical parameterizations of vertical transport – start to unveil the remarkably rich dynamics of thermohaline intrusions. Simulations have become more reliable and realistic. The observational database of interleaving accumulated in numerous field programs is already impressive, covering various forms of interleaving and geographic locations. These positive trends can only accelerate in the future as the significance of interleaving becomes more and more evident.

What seems to be lagging at the moment is our ability to link the interleaving theory with field measurements. Some problems are temporary. As we get wiser and better understand the relevant dynamics, we will find new ways to diagnose and interpret oceanographic observations. Other barriers could be more fundamental and related to the limited predictability of any turbulent environment. In view of these challenges, I would like to close this chapter with an (incomplete) list of considerations that should be taken into account in order to bring intrusion theories into agreement with observations:

(i) Intrusion characteristics are affected by the (less predictable) small-scale turbulence due to overturning gravity waves in the ocean; the turbulent component is spatially inhomogeneous and often controlled by external factors, such as topography and tidal forcing.
(ii) The instantaneous measurements of intrusions may reflect conditions that existed in the past history of a thermohaline front.

(iii) Secondary sub-harmonic instabilities of intrusions can lead to merging events, systematically increasing their vertical scale.

(iv) Intrusive perturbations could be initiated by processes unrelated to double-diffusion but maintained and enhanced by fundamentally thermohaline processes. In this case, the selective advantage of the most rapidly growing modes may be insufficient to ensure their dominance in the fully developed state.

(v) Significant uncertainties still exist in the formulation of the flux-gradient laws – the key element of parametric models. The effects of background shear, intermittent turbulence and internal waves on the salt-finger transport are typically not taken into account and can be substantial.